A TWO-DIMENSIONAL PHOTONIC CRYSTAL FOR SURFACE TEMPERATURE MAPPING

by

DURDU GUNEY

Submitted to the Graduate School of Engineering and Natural Sciences

in partial fulfillment of

the requirements for the degree of

Master of Science

Sabancı University

Spring 2002

To My Family,

vermiş oldukları emeğin karşılığını ödeme temennisi ile…

*"… Τηε Παραβλε οφ Ηισ Λιγητ ισ ασ ιφ τηερε ωερε α Νιχηε ανδ ωιτηιν ιτ α Λαμπ: τη
ε Λαμπ ενχλοσεδ ιν Γλασσ: τηε γλασσ ασ ιτ ωερε α βριλλιαντ σταρ: Λιτ φρομ α βλεσ
σεδ Τρεε, αν Ολιῶε, νειτηερ οφ τηε εαστ νορ οφ τηε ωεστ, ωηοσε οιλ ισ ωελλ–νιγη λυ
μινουσ, τηουγη φιρε σχαρχε τουχηεδ ιτ: Λιγητ υπον Λιγητ! … "*

ACKNOWLEDGEMENT

A TWO-DIMENSIONAL PHOTONIC CRYSTAL FOR SURFACE TEMPERATURE MAPPING

ABSTRACT

A two-dimensional photonic band gap structure is proposed for surface temperature reading of objects. Optical properties of GaAs are utilised in the design and simulation of the device since GaAs is nearly transparent and lossless in the chosen infrared region, and also has a reasonably high dielectric constant of 11.4. The structure consists of a triangular lattice of air holes etched into a GaAs slab, with a lattice constant, a, of 0.382 μm, including one linear waveguide and three isolated point defects with radii $0.51a$, $0.54a$, and $0.57a$, respectively. The operational principle of the device is based on guiding and vertically filtering out three pre-selected specifically tuned wavelengths through the corresponding point defects. It is shown that having processed the intensities of these wavelengths, obtained from each defect, in accordance with the blackbody radiation characteristics and the transmission properties of the device, the temperature reading of the target in concern is obtained.

ÖZET

Objelerin yüzey sıcaklıklarını tespit edebilmek amacıyla iki-boyutlu fotonik kristal önerilmiştir. Bu kristal yapısının dizaynı ve simülasyonu sırasında kullanacağımız dalgaboyunun kristali saydam kılmasına ve icinde enerji kaybına yol açmamasına dikkat edilmiştir. Bu nedenle ışık spektrumunun kızılötesi bölgesinde tamamen saydam ve soğurma özelliği göstermeyen GaAs seçilmiştir. GaAs seçilmesinin bir diğer sebebi de 11.4 gibi oldukça büyük dielektrik sabitine sahip olmasıdır. Çünkü dielektrik kontrastının fazla olması kullanacağımız fotonik band aralığını da genişletmektedir. Kullandığımız kristal yapısı temel olarak hava sütunlarinin üçgensel bir biçimde GaAs içine gömüldüğü tabakadan oluşmakta olup ayrıca belli bir sıradaki hava sütunları oluşturulmayarak böylece o yönde bir dalgakılavuzu oluşturulmuştur. Dalgakılavuzunun hemen yakınlarına ise izole edilmiş noktasal düzensizlikler (point defect) yerleştirilmiştir. Oluşan kristal yapısının latis sabiti, a, 0.382 µm, ve noktasal düzensizliklerin yarıçapları ise sırasıyla $0.51a$, $0.54a$ ve $0.57a$ olarak alınmıştır. Dizaynı yapılan aletin çalışma prensibi, önceden belirlenmiş olan belli bir frekans bandının aletin içinde oluşturulmuş olan dalgakılavuzu ile taşınıp noktasal düzensizliklerden bu band içindeki belli rezonant frekansların filtrelenmesi temeline dayanmaktadır. Rezonant frekansları önceden kendimiz belirleyerek aleti ona göre tasarlayabiliriz. Daha sonra, rezonant frekanslardan elde edilen elektromanyetik gücün analizi, karacisim ışıması ve kullandığımız aletin optik özellikleri yardımı ile hedefteki objenin yüzey haritası çıkartılabilmektedir.

TABLE OF CONTENTS

LIST OF FIGURES

1. INTRODUCTION

Many of the true breakthroughs have resulted from a deeper understanding of the properties of materials.

In this century, our control over materials has spread to include their *electrical* properties. Advances in semiconductor physics have allowed us to tailor the conducting properties of certain materials, thereby initiating the transistor revolution in electronics.

In the last decade a new frontier has emerged with a similar goal: to control the *optical* properties of materials. If we could engineer materials that prohibit the propagation of light, or allow it only in certain directions at certain frequencies, or localize light in specified areas, our technology would benefit. Already, fiber-optic cables, which simply guide light, have revolutionized the telecommunications industry. Lasers, high-speed computers are just a few of the fields next in line to reap the benefits from the advances in optical materials. It is with this goal in mind that this work has been done.

In particular, the lattice might introduce gaps into the energy band structure of the crystal, so that electrons are forbidden to propagate with certain energies in certain directions. If the lattice potential is strong enough, the gap might extend to all possible directions, resulting in a *complete band gap*. For example, a semiconductor has a complete band gap between the valence and conduction energy bands.

The optical analogy is the *photonic* crystal, in which the periodic "potential" is due to a lattice of macroscopic dielectric media instead of atoms. If the dielectric constants of the materials in the crystal are different enough, and the absorption of light by the material is minimal, then scattering at the interfaces can produce many of the same phenomena for *photons* (light modes) as the atomic potential does for *electrons*. The solution to the problem of optical control and manupulation is thus a *photonic crystal*, a low-loss periodic dielectric periodic medium. In particular, we can design and construct photonic crystals with *photonic band gaps*, preventing light from propagating in certain directions with specified energies.

Photonic crystals cannot only mimic the properties of cavities and waveguides but are also scalable and applicable to a wider range of frequencies. We may construct a photonic crystal with millimeter dimensions for microwave control, or with micron dimensions for infrared control.

The aim of this introduction is to provide a comprehensive description of the propagation of light in photonic crystals.

In chapter 2, I will make a a brief review of photonic band gap materials and physics behind. First I will make a physical modeling of photonic crystals using the Maxwell equations in a mixed dielectric media, which is the more general case. Photonic crystals apply to more specific type of mixed dielectric media, where the dielectric regions in the medium alternate in various directions periodically. It is clear that because the photonic crystal domain in this problem can be considered as a subset of mixed dielectric medium, the mathematical modeling developed in chapter 2 also applies to all kinds of photonic crsytals, indeed. The necessary assumptions in this model are briefly introduced, and they are carefully chosen in order not to lack the viability of the model for all kinds of photonic crystals to be realized in real life.

Then I go through the symmetry properties of photonic crystals. As in the many electromagnetic problems, symmetry considerations play a critical role in the algorithms, which are developed to solve those problems. Because the symmetry arguments simplify the algorithms, it requires less computational power. For example, in the photonic crystal computations, which I performed throughout this thesis project, I used mainly two

electromagnetic algorithms: Plane-wave Expansion Method (PEM) and Finite Difference Time Domain Method (FDTD). Both of this electromagnetics methods are rather susceptible to the symmetry arguments. Thus, it is in this context thought to mention the symmetry in chapter 2. It must also be mentioned that in the calculation of photonic band structure, the classification of electromagnetic modes into transverse-electric (TE) and transverse-magnetic (TM) plays a crucial role. Only in this way it is possible to examine the polarization characteristics of the structure studied, which lead to many interesting phenomena in the literature.

I will describe the properties of photonic crystals of gradually increasing complexity - beginning with one-dimensional crystals and moving on to the more intricate and useful properties of two- and a little bit three- dimensional systems. Perfect photonic crystals of one- two- and three- dimensions are illustrated in figure 1.1. The word perfect, here, expresses the meaning that the crystals extends infinity in the directions which are not periodic along. In other words, perfect photonic crystals are not the real world phenomena, they can only be considered to explain the physics behind but, nevertheless, they are extremely powerful to explain the physics of the practical photonic crystal slabs. There are several methods to pass from the perfect crystals to slabs, such as including light cone and the effective refractive index method. While proceeding, I begin to address pragmatic questions: which structures yield what properties, and why?
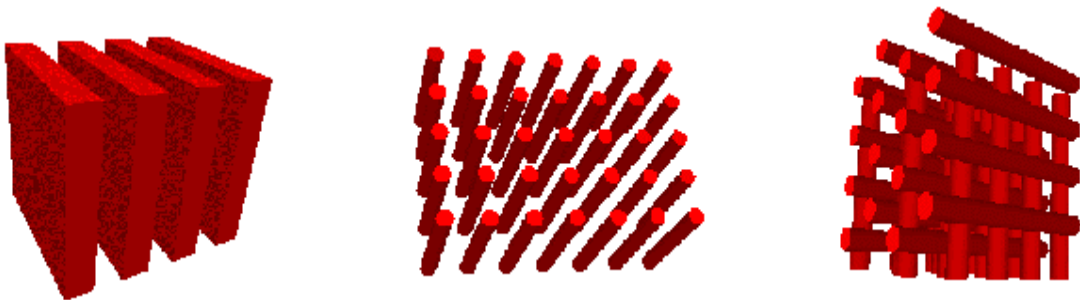
Figure 1.1 Geometry of one-, two-, and three- dimensional photonic crystals.

After addressing the many useful proerties of photonic band gap materials, I compare the electromagnetic band gap which ocurs in the semiconductors with the photonic band gap which opens up in the photonic crystals. We will realize that photonic crystals are analogous

to semiconductors, which manifest stop-band for photons with a certain range of frequency band.

After all, I will mention the work of Noda et al [1], published in Nature (2000), from which I get much enlightenment for my project and made fruitful discussion with one of the authors.

And finally, in chapter 3, I describe my thesis project. Some conclusions and suggestions for future work are also included.

2. THEORY OF PHOTONIC CRYSTALS

2.1 Maxwell Equations as a Linear Hermitian Eigenvalue Problem

In order to study the propagation of light in a photonic crystal, we must turn to the Maxwell equations. After specialising to the case of a mixed dielectric, we will express the Maxwell equations as a linear Hermitian eigenvalue problem. From this formulation, in close anology, with the Schrodinger equation of quantum mechanics, comes a variety of useful properties, including the orthogonality of modes and the electromagnetic variational theorem. Finally, I will show how the electromagnetic problems with different overall length and dielectric scales can be related.

The propagation of light in photonic crystal is governed by the four macroscopic Maxwell equations:

$$\nabla \cdot \mathbf{B} = 0 \qquad\qquad \nabla \times \mathbf{E} + 1/c\ \partial\mathbf{B}/\partial t = 0 \qquad\qquad 2.1.1$$

$$\nabla \cdot \mathbf{D} = 4\pi\rho \qquad\qquad \nabla \times \mathbf{H} - 1/c\ \partial\mathbf{D}/\partial t = 4\pi/c\ \mathbf{J}. \qquad\qquad 2.1.2$$

We will restrict ourselves to propagation within a *mixed dielectric medium*. With this type of medium in mind, in which light propagates but there are no sources of light, we can set $\rho = \mathbf{J} = 0$.

For many dielectric materials, it is a good approximation to employ the following standard assumptions. First, we assume the field strengths are small enough. Second, we assume the material is macroscopic and isotropic. Third, we ignore any explicit frequency dependence of the dielectric constant. Fourth, we focus only on low-loss dielectrics, which means we can treat $\varepsilon(\mathbf{r})$ as purely real.

When all is said and done, we have $\mathbf{D}(\mathbf{r}) = \varepsilon(\mathbf{r})\mathbf{E}(\mathbf{r})$. For most dielectric materials of interest, the magnetic permeability is very close to unity and we may set $\mathbf{B} = \mathbf{H}$.

In general both $\mathbf{E}$ and $\mathbf{H}$ are complicated functions of time and space. But since the Maxwell equations are linear, we can separate out the time dependence by expanding the fields into a set of harmonic modes. So we will concern ourselves with the restrictions that the Maxwell equations impose on a field pattern that happens to vary harmonically with time. This is no great limitation, since we know by Fourier analysis that we can build *any* solution with an appropriate combination of these harmonic modes.

For mathematical convenience we will write a harmonic mode as a certain field pattern times a complex exponential:

$$\mathbf{H}(\mathbf{r}, t) = \mathbf{H}(\mathbf{r})e^{i\omega t} \qquad\qquad 2.1.3$$

$$\mathbf{E}(\mathbf{r}, t) = \mathbf{E}(\mathbf{r})e^{i\omega t} . \qquad\qquad 2.1.4$$

To find the equations for the mode profiles of a given frequency, we insert the above equations into the Maxwell equations using also the constitutive relations. From the divergence equations we find that the field configurations are built up of *transverse* electromagnetic waves. That is, if we have a plane wave $\mathbf{H}(\mathbf{r}) = \mathbf{a}\,\exp(i\mathbf{k}.\mathbf{r})$, then $\mathbf{a} \cdot \mathbf{k} = 0$. Furthermore, from the curl equations we can get the following equation entirely in $\mathbf{H}(\mathbf{r})$:

$$\nabla \times [\ 1/\varepsilon(\mathbf{r})\ \nabla \times \mathbf{H}(\mathbf{r})] = (\omega/c)^2\ \mathbf{H}(\mathbf{r}). \qquad\qquad 2.1.5$$

This is the master equation. In addition to the divergence equations, it completely determines $\mathbf{H}(\mathbf{r})$ and then $\mathbf{E}(\mathbf{r})$ can also be solved.

We identify the left side of the master equation as an operator Θ acting on $\mathbf{H}(\mathbf{r})$ to make it look explicitly like an eigenvalue problem:

$$\Theta\, \mathbf{H}(\mathbf{r}) = (\omega/c)^2\, \mathbf{H}(\mathbf{r}). \qquad\qquad 2.1.6$$

The eigenvectors $\mathbf{H}(\mathbf{r})$ are the field patterns of the harmonic modes, and the eigenvalues $(\omega/c)^2$ are proportional to the squared frequencies of those modes. One important thing to notice is that the operator Θ is a linear operator. That is, any linear combination of solutions is itself a solution; if $\mathbf{H}_1(\mathbf{r})$ and $\mathbf{H}_2(\mathbf{r})$ are both solutions to this eigenvalue equation with the same frequency ω, then so is $\alpha\mathbf{H}_1(\mathbf{r}) + \beta\mathbf{H}_2(\mathbf{r})$, where α and β are constants. For example, given a certain mode profile, we can construct another legitimate mode profile with the same frequency by simply doubling the field strength everywhere ($\alpha = 2$, $\beta = 0$). For this reason we consider two field patterns that differ only by an overall multiplier to be essentially the same mode.

Our operator notation is reminiscent of quantum mechanics, in which we obtain an eigenvalue equation by operating on the wave function with the Hamiltonian. We might recall from quantum mechanics some key properties of the eigenfunctions of the Hamiltonian: they have real eigenvalues, they are orthogonal, and may be catalogued by their symmetry properties.

All of these same useful properties hold for our formulation of electromagnetism. In both cases, the properties rely on the fact that the main operator is a special type of linear operator known as a *Hermitian* operator.

Because Θ is Hermitian, it can be shown that Θ must have real eigenvalues and it follows that ω^2 is real and positive.

Additionally, the Hermiticity of Θ forces any two harmonic modes $\mathbf{H}_1(\mathbf{r})$ and $\mathbf{H}_2(\mathbf{r})$, with frequencies ω_1 and ω_2:

$$\omega_1{}^2(\mathbf{H}_2,\mathbf{H}_1) = c^2(\mathbf{H}_2,\Theta\mathbf{H}_1) = c^2(\mathbf{H}_1,\Theta\mathbf{H}_2) = \omega_2{}^2(\mathbf{H}_2,\mathbf{H}_1)$$
$$\rightarrow (\omega_1{}^2 - \omega_2{}^2)(\mathbf{H}_2,\mathbf{H}_1) = 0. \qquad\qquad 2.1.7$$

If $\omega_1 \neq \omega_2$, then we must have $(\mathbf{H}_1, \mathbf{H}_2) = 0$ and we say $\mathbf{H}_1$ and $\mathbf{H}_2$ are *orthogonal* modes. If two harmonic modes have equal frequencies $\omega_1 = \omega_2$, then we say they are *degenerate* and they are not necessarily orthogonal. For two modes to be degenerate requires what seems to be an astonishing coincidence: two different field patterns that to have precisely the same frequency. Usually there is a symmetry that is responsible for the "coincidence." For example, if the dielectric configuration is invariant under a 120° rotation, modes that differ only by a 120° rotation are expected to have the same frequency, such modes are degenerate and are not necessarily orthogonal.

Although the harmonic modes in a dielectric medium can be quite complicated, there is a simple way to understand some of their qualificative features. Roughly, a mode tends to concentrate its displacement energy in regions of high dielectric constant, while remaining orthogonal to the modes below it in frequency. This intiutive notion finds expression in the *electromagnetic variational theorem*. The lowest-frequency mode, for instance, is the field pattern that minimizes the electromagnetic energy functional [2]:

$$E_{\mathrm{f}}(\mathbf{H}) = (\mathbf{H}, \Theta \mathbf{H}) / 2(\mathbf{H}, \mathbf{H}). \qquad\qquad 2.1.8$$

Careful considerations show that the lowest electromagnetic eigenmode, $\mathbf{H}_0$, will *minimize E_{f}*. The next lowest eigenmode will minimize E_{f} in the subspace orthogonal to $\mathbf{H}_0$, and so on.

Using the electomagnetic energy functional it can be shown that

$$E_{\mathrm{f}}(\mathbf{H}) = (\smallint d\mathbf{r}\ \varepsilon^{-1}\ |\omega\mathbf{D}/\mathrm{c}|^2\ ) / 2(\mathbf{H}, \mathbf{H}). \qquad\qquad 2.1.9$$

From this expression we can see that E_{f} is minimized when the displacement field $\mathbf{D}$ is concentrated in the regions of high dielectric constant. To minimize E_{f}, a harmonic mode will therefore tend to concentrate its displacement field in regions of high dielectric, while remaining orthogonal to the modes below it in frequency.

In addition to the variational energy functional, two other important energies of an electromagnetic system are the *physical* energies stored in the electric and magnetic fields:

$$E_D = (1/8\pi) \int d\mathbf{r} \; \varepsilon^{-1}(\mathbf{r})|\mathbf{D}(\mathbf{r})|^2 \qquad\qquad 2.1.10$$

$$E_H = (1/8\pi) \int d\mathbf{r} \; |\mathbf{H}(\mathbf{r})|^2. \qquad\qquad 2.1.11$$

For a harmonic mode, we can show that $E_D = E_H$, so that as time passes the field energy is harmonically exchanged between the displacement and magnetic fields. Although E_f and E_D have similar form, there is a very important difference. The energy functional has a normalizing term in the denominator and allows us to characterize the electromagnetic modes independent of the field strength. The physical energy stored in the electric field, on the other hand, is proportional to the square of the field strength. In other words, if we are interested in the physical energies, we cannot just normalize our fields, but if we are only interested in mode patterns, overall multipliers are irrelevant.

One interesting feature of electromagnetism in dielectric media is that there is no fundamental length scale other than assumption that the system is macroscopic. If we want to know the new mode profile after changing the length scale by a factor s, $\mathbf{r} \to s\mathbf{r}$, we just scale the old mode and its frequency by the same factor, $\omega \to \omega/s$. The solution of the problem at one length scale determines the solutions for all other length scales.

This simple fact is of considerable practical importance. For example, the microfabrication of complex micron-scale photonic crystals can be quite difficult. But models can be easily made and tested in the microwave regime, at the much larger length scale of centimeters. The model wil have the same electromagnetic properties.

Just as there is no fundamental *length* scale, there is no fundamental value of the dielectric constant. Suppose we know the harmonic modes of a system with a dielectric configuration $\varepsilon(\mathbf{r})$, and we are curious about the modes of a system with a dielectric configuration that differs by a constant factor everywhere, so that $\varepsilon'(\mathbf{r}) = \varepsilon(\mathbf{r})/s^2$. The harmonic modes of the new system are unchanged , but the frequencies are all scaled by a factor s: $\omega \to \omega' = s\omega$. If we multiply the dielectric constant everywhere by a factor of $1/4$, the mode patterns are unchanged but their frequencies double.

2.2 Symmetries for the Classification of Electromagnetic Modes

A system that has continous translational symmetry in *all three* directions in free space: $\varepsilon(\mathbf{r}) = 1$. It can be deduced from the symmetry arguments [2] that the modes must have the form

$$\mathbf{H_k(r)} = \mathbf{H}_0\, e^{i(\mathbf{k.r})}, \qquad\qquad 2.2.1$$

Where $\mathbf{H}_0$ is any constant vector. These are just plane waves, polarized in the direction of $\mathbf{H}_0$. Imposing the transversality requirement gives the further restriction $\mathbf{k.H}_0 = 0$. We can also verify that these plane waves are in fact solutions of the master equation with eigenvalues $(\omega/c)^2 = k^2$. We classify plane waves by specifying $\mathbf{k}$, which specifies how the mode behaves under a translation operation.

Photonic crystals, like the familiar crystals of atoms, do not have continous translational symmetry; instead they have *discrete* translational symmetry. That is, they are not invariant under translations of *any* distance -only under distances that are multiple of some fixed step length. The simplest example of such a system is a structure that is repetitive in one direction, like the one-dimensional configuration in figure 2.2.1. The structure consists of alternating layers of high (red) and low (here, air) dielectric layers. In the figure yellow-bordered box describes the unit cell and the distance between each unit cell is defined as the *lattice constant* as in the semiconductor physics.

For this system we still have continous translational symmetry in the *x*-direction, but now we have discrete translational symmetry in the *y*-direction. The basic step-length is the lattice constant, *a*, and the basic step vector is called the *primitive lattice vector*; which in this case is $\mathbf{a} = a\mathbf{y}$ ($\mathbf{y}$ is the unit vector in the *y*-direction). Because of the symmetry, $\varepsilon(\mathbf{r}) = \varepsilon(\mathbf{r} + \mathbf{a})$. By repeating this translation, we see that $\varepsilon(\mathbf{r}) = \varepsilon(\mathbf{r} + \mathbf{R})$ for any $\mathbf{R}$ that is an integral multiple of $\mathbf{a}$; that is, $\mathbf{R} = l\mathbf{a}$, where *l* is an integer.

The dielectric unit that we consider to be highlighted in the figure with the box, is known as the *unit cell*.

We can classify the modes by specifying k_x and k_y. However, not all the values of k_y yield different eigenvalues. In fact, all of the modes with wavevectors of the form $k_y + m(2\pi/a)$,

where m is an integer, form a degenerate set; they all have the same eigenvalue. Augmenting k_y by an integral multiple of $b = 2\pi/a$ leaves the state unchanged. We call $\mathbf{b} = b\mathbf{y}$ the primitive *reciprocal* lattice vector.

Since any linear combination of these degenerate eigenfunctions is itself an eigenfunction with the same eigenvalue, we can take linear combinations of our original modes to put them in the form

$$\mathbf{H}_{kx,\,ky}(\mathbf{r}) = e^{ik_x x} \, \boldsymbol{\Sigma}_m \, \mathbf{c}_{ky,\,m}(z) \, e^{i(k_y + mb)\,y} = e^{ik_x x} \, e^{ik_y y} \, \boldsymbol{\Sigma}_m \, \mathbf{c}_{ky,\,m}(z) \, e^{imby} = e^{ik_x x} . e^{ik_y y} . \mathbf{u}_{ky}(y,z) \qquad 2.2.2$$

where c's are expansion coefficients to be determined by explicit solution, and $\mathbf{u}(y,z)$ is a periodic function in y. We can verify that $\mathbf{u}(y+la,\,z) = \mathbf{u}(y,z)$. This result is commonly known as *Bloch's theorem* [2].

One key fact about the Bloch states is that Bloch state with wave vector $k_y + mb$ are identical. The k_y's that differ by integral multiples of $b = 2\pi/a$ are not different from a physical point of view. Thus the mode frequencies must also be periodic in k_y: $\omega(k_y) = \omega(k_y + mb)$. In fact only need to consider k_y exist in the range $-\pi/a < k_y \le \pi/a$. This region of important, nonredundant values of k_y is called the *Brillouin zone*.

The Brillouin zone for the structure in figure 2.2.1 can be considered the same as the structure itself, but in *k*-space. Thus, if we coincide both spaces we can say that yellow-bordered box corresponds to first Brillouin zone, again as in the solid state physics. However, the irreducible Brillouin zone is indeed the half of this box, which contains the all possible wavevectors allowed in the structure, as explained in the previous paragraph.

We digress briefly to make analogous arguments that apply when the dielectric is periodic in three dimensions. In this case the dielectric is invariant under translations through a multitude of lattice vectors $\mathbf{R}$ in three dimensions. Any one of these lattice vectors can be written as a particular combination of three primitive lattice vectors ($\mathbf{a}_1$, $\mathbf{a}_2$, $\mathbf{a}_3$) that are said to 'span' the space of lattice vectors. In other words, every $\mathbf{R} = l\mathbf{a}_1 + m\mathbf{a}_2 + n\mathbf{a}_3$ for some integers l, m, and n. The vectors ($\mathbf{a}_1$, $\mathbf{a}_2$, $\mathbf{a}_3$) give rise to three primitive *reciprocal* lattice vectors ($\mathbf{b}_1$, $\mathbf{b}_2$, $\mathbf{b}_3$)

defined so that $\mathbf{a}_i \cdot \mathbf{b}_j = 2\pi\delta_{ij}$. These reciprocal vectors form a lattice of their own which is inhabited by wave vectors.
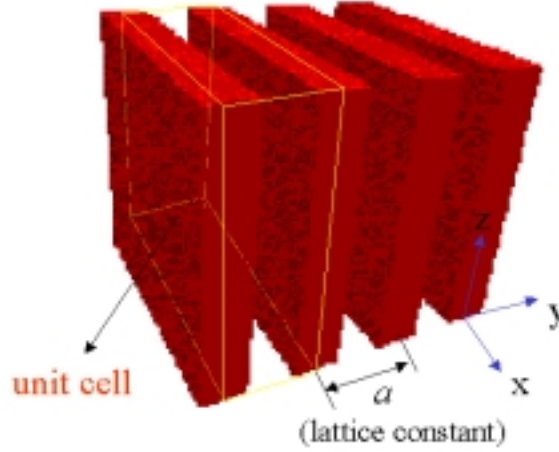
Figure 2.2.1 Discrete translational symmetry in one-dimensional multilayer film.

The modes of a three dimensional periodic system are Bloch states that can be labeled by $\mathbf{k} = k_1\mathbf{b}_1 + k_2\mathbf{b}_2 + k_3\mathbf{b}_3$, where $\mathbf{k}$ lies in the Brillouin zone. Each value of the wave vector $\mathbf{k}$ inside the Brillouin zone identifies an eigenstate of Θ with frequency $\omega(\mathbf{k})$ and eigenvector $\mathbf{H_k}$ of the form

$$\mathbf{H_k}(\mathbf{r}) = e^{i\,(\mathbf{k}.\mathbf{r})}\,\mathbf{u_k}(\mathbf{r}), \qquad\qquad 2.2.3$$

where $\mathbf{u_k}(\mathbf{r})$ is a periodic function on the lattice: $\mathbf{u_k}(\mathbf{r}) = \mathbf{u_k}(\mathbf{r} + \mathbf{R})$ for all lattice vectors $\mathbf{R}$.

Since $\mathbf{k}$ enters only as a parameter in Θ, we expect the frequency of each band, for given $\mathbf{k}$, to vary continously as $\mathbf{k}$ varies. In this way we arrive at the description of the modes of a photonic crystal. They are a family of continous functions, $\omega_n(\mathbf{k})$, indexed in order of increasing frequency by the band number. The information contained in these functions is called the *band structure* of the photonic crystal. Studying the band structure of a crystal supplies us with most of the information we need to predict its optical properties.

Photonic crystals might have symmetries other than discrete translations. A given crystal might also be invariant after rotation, a mirror reflection, or an iversion.

12

It can be derived from the *rotational* symmetry arguments [2] that

$$\omega_n(\Re\mathbf{k}) = \omega_n(\mathbf{k}).$$ 2.2.4

We conclude that when there is rotational symmetry in the lattice, the frequency bands $\omega_n(\mathbf{k})$ have additional redundancies within the Brillouin zone. In a similar manner, it can be shown that whenever a photonic crystal has a rotation, mirror-reflection, or inversion symmetry, the $\omega_n(\mathbf{k})$ functions have that symmetry as well. This particular collection of symmetry operations (rotations, reflections, and inversions) is called the *point group* of the crystal.

Since $\omega_n(\mathbf{k})$ possess the full symmetry of the point group, we need not consider them at every $\mathbf{k}$-point in the Brillouin zone. The smallest region within the Brillouin zone for which the $\omega_n(\mathbf{k})$ are not related by symmetry are is called the *irreducible* Brillouin zone. The *irreducible* zone is a triangular wedge with 1/8 the area of the full Brillouin zone; the rest of the Brillouin zone contains the redundant copies of the irreducible zone.

Furthermore, mirror reflection symmetry in a photonic crystal deserves special attention. Under certain conditions it allows us to separate the eigenvalue equation for Θ into two separate equations, one for each field polarization. In one case $\mathbf{H_k}$ is perpendicular to the mirror plane and $\mathbf{E_k}$ is parallel; while in the other case, $\mathbf{H_k}$ is in the plane and $\mathbf{E_k}$ is perpendicular. This simplification is convenient, because it provides immediate information about the mode symmetries and also facilitates the numerical calculation of their frequencies.

Two-dimensional photonic crystals are periodic in a certain plane, but are uniform along an axis perpendicular to that plane. Calling that axis the *z*-axis, we know that the operation $\mathbf{z} \rightarrow -\mathbf{z}$ is a symmetry of the crystal for any choice of origin. It also follows that $M_z\mathbf{k}_{//} = \mathbf{k}_{//}$ for all wave vectors in the $\mathbf{k}_{//}$ in the two-dimensional Brillouin zone. Thus the modes of *every* two-dimensional photonic crystal can be classified into two distinct polarizations: (either E_x, E_y, H_z) or (H_x, H_y, E_z). The former in which the *electric* field is confined to the *xy*-plane, are called transverse-electric (TE) modes. The latter, in which the *magnetic* field is confined to the *xy*-plane, are called transverse-magnetic (TM) modes.

On the other hand, it can also be shown from the complex conjugation arguments [2] that

$$\omega_n(\mathbf{k}) = \omega_n(-\mathbf{k}). \qquad 2.2.5$$

This relation holds for *any* photonic crystal. Taking the complex conjugate of $\mathbf{H}_{\mathbf{k}n}$ is equivalent to reversing the sign of time *t* in the Maxwell equations. For this reason, we say that this relation is a consequence of the *time-reversal* symmetry of the Maxwell equations.

2.3 One-Dimensional Photonic Crystals

The simplest possible photonic crystal consists of alternating layers of material with dielectric constants. This arrangement is not a new idea -the optical properties of such *multilayer films* have been widely studied.
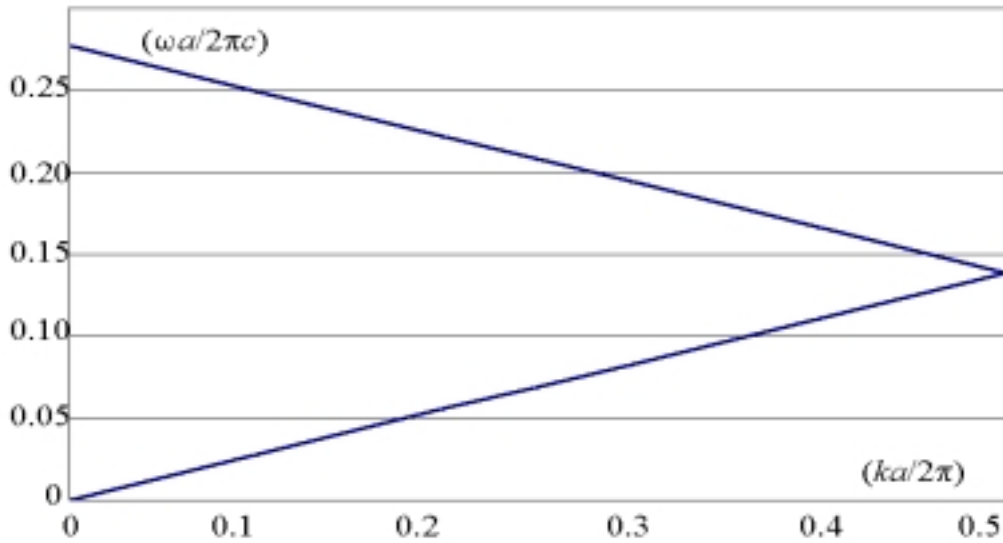
Figure 2.3.1 Photonic band structure of a homogeneous GaAs medium.

We can write the modes in the Bloch form

$$\mathbf{H}_{n,kz,\mathbf{k}//}(\mathbf{r}) = e^{i\mathbf{k}//\cdot\boldsymbol{\rho}}e^{ik_z z}\,\mathbf{u}_{n,kz,\mathbf{k}//}(z). \qquad 2.3.1$$

Here, $\mathbf{u}(z)$ is a *z*-periodic function, so that $\mathbf{u}(z) = \mathbf{u}(z+R)$ whenever *R* is an integral multiple of *a*, the layer spacing. The crystal has continous translational symmetry in the *xy*-plane, so the

$\mathbf{k}_{//}$ can assume any value. However, we restrict k_z to finite interval, the one-dimensional Brillouin zone, because the crystal has discrete translational symmetry in the z-direction.

For now, consider light that happens to propagate entirely in the z-direction, crossing the sheets of dielectric at normal incidence. In this case, $\mathbf{k}_{//} = 0$, so only the wave vector component k_z is important. Without possibility of confussion, we can abbreviate k_z by k.

In figures 2.3.1, 2, and 3, $\omega_n(k)$ is plotted for three different multilayer films. In figure 2.3.1, all of the strips have the same dielectric constant, so the medium is completely homogeneous. This is nothing more than the dispersion relation for a homogeneous dielectric medium. However, figure 2.3.2 is for a structure with alternating dielectric constants of 13 and 12, note that a very slight gap opens up in this figure due to the index contrast we introduced. That is the band gap which our interest is based on. In figure 2.3.3 is shown the band structure for a structure with a much higher dielectric contrast of 13 to 1. It is clear from these figures that the more index contrast is introduced, the larger band gap we obtain.
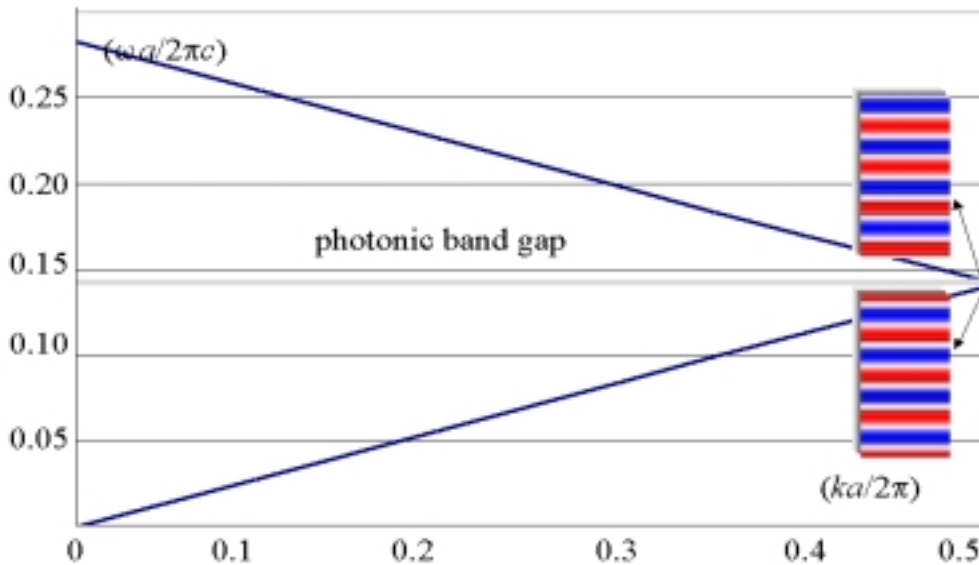
Figure 2.3.2 Photonic band structure of a multilayer film with an index ratio of 13:12.

There is a frequency gap in frequency between upper and lower branches of the lines -a frequency gap in which no mode, regardless of k, can exist in the crystal. We call such a gap a *photonic band gap*.

The natural question arises: Why does the photonic band gap appear? We can understand the gap's physical origin by cosidering the electric field mode profiles for the states immediately *above* and *below* below the gap. For $k = \pi/a$, the modes are standing waves with a wavelength of $2a$, twice the crystal's lattice constant.

There are two ways to center a standing wave of this type. We can position its nodes in each low-ε layer or in each high-ε layer. The calculated spatial pattern of displacement field is shown in the insets of figure 2.3.2. Any other position would violate the symmetry of the unit cell about its center.
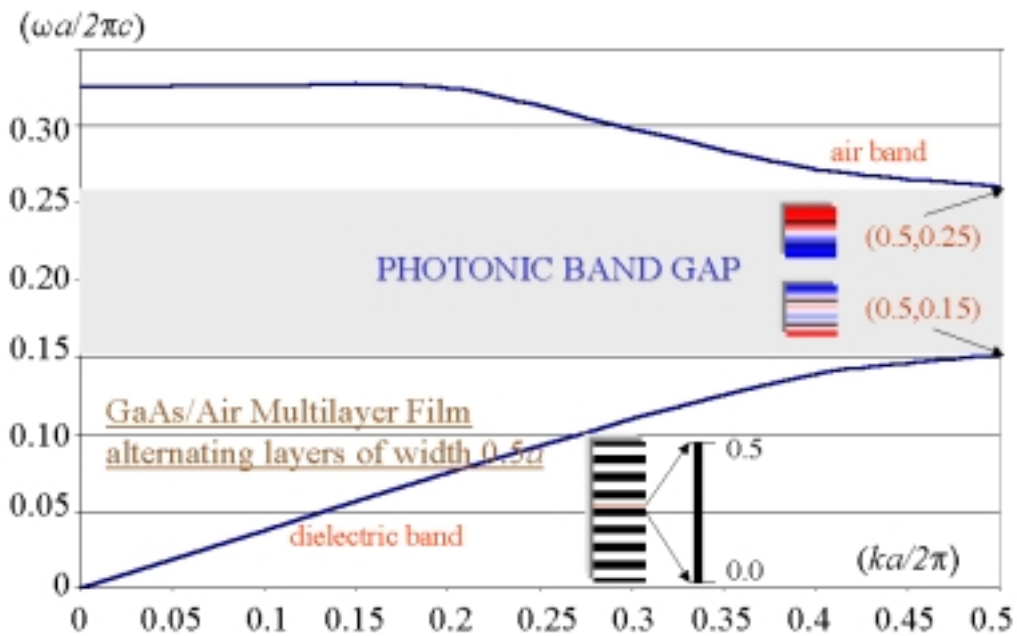
Figure 2.3.3 Photonic band structure of a multilayer film with an index ratio of 13:1.

As in our previous discussions of electromagnetic variational theorem, the low-frequency modes concentrate their energy in the high-ε regions, and the high-frequency modes concentrate their energy in the low-ε regions. With this in mind, it is understandable why there is a frequency difference between the two cases. The mode just *under* the gap has its power concentrated in the $\varepsilon = 13$ regions as shown in the lower inset of figure 2.3.2, giving it a lower frequency. Meanwhile, the mode just above the gap has most of its power in lower $\varepsilon = 12$ regions as shown in the upper inset of figure 2.3.2, so its frequency is raised a bit. The

mid-layer in the insets (showing the power distribution) of figure 2.3.2 corresponds to low dielectric layer.

The bands above and below the gap can be distinguished by where the power of their modes lies. Often the low-ε regions are air regions. For this reason, it is convenient to refer to the band *above* a photonic band gap as the "air band," and the band *below* a gap as the "dielectric band". The situation is analogous to the electronic band structure of semiconductors, in which the "conduction band" and the "valence band" surround the fundamental gap.

When we say that there are no states in the photonic band gap, it is meant that there are no *extended* states in the photonic band gap. Instead, the modes are *evanescent*, decaying exponentially:

$$\mathbf{H}(\mathbf{r}) = e^{ikz}\mathbf{u}(z)e^{-\kappa z}. \qquad\qquad 2.3.2$$

They are just like the extended modes, but with a complex wave vector $k+i\kappa$. The imaginary component of the wavevector causes the decay. We would like to understand how these evanescent modes originate and what determines κ. This can be accomplished by examining the bands in the immeadiate vicinity of the gap. Return to figure 2.3.3. Suppose we try to approximate the second band near the gap by expanding $\omega_2(k)$ in powers of k about the zone edge $k = \pi/a$. Because of time-reversal symmetry, the expansion cannot contain odd powers of k, so to lowest order:

$$\Delta\omega = \omega_2(k) - \omega_2(\pi/a) = \alpha(k\text{-}\pi/a)^2 = \alpha(\Delta k)^2. \qquad\qquad 2.3.3$$

Now we can see where the complex wave vector originates. For frequencies slightly higher than the top of the gap, $\Delta\omega > 0$. In this case, Δk is purely real, and we are within band 2. However, for $\Delta\omega < 0$, when we are within the gap, Δk is purely imaginary. The states decay exponentially since $\Delta k = i\kappa$. As we traverse the gap, the decay constant κ grows as the frequency reaches the gap's center, then disappears at the lower edge. This behaviour is depicted in figure 2.3.4.
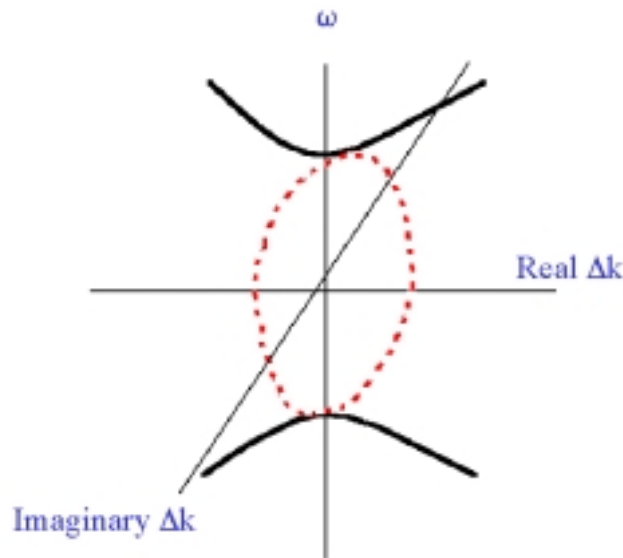
Figure 2.3.4 Description of evanescent modes.

We should emphasize that although evanescent modes are genuine solutions of the eigenvalue problem, they do not satisfy the translational-symmetry boundary condition of the crystal. There is no way to excite them in a perfect crystal of infinite extent. However, a defect or an edge in an otherwise perfect crystal might sustain such a mode.

So far we have considered the modes of a one-dimensional photonic crystal which happen to have $\mathbf{k}_{//} = 0$; that is, modes that propagate only in the z-direction. Figure 2.3.3 shows the band structure for modes with $\mathbf{k} = k_y\mathbf{y}$.

The most important difference between on-axis and off-axis propagation is that there are *no band gaps* for off-axis propagation when all possible k_y are considered. This is always the case for a multilayer film, because the off-axis direction contains no periodic dielectric regions to coherently scatter the light and split open a gap.

Another difference involves the *degeneracy* of the bands. For on-axis propagation, the electric field is oriented in the *xy*-plane. We might choose the two-basic polarizations as the *x*- and *y*-directions. Since those two modes polarizations differ only by a rotational symmetry which the cystal possesses, they must be degenerate.
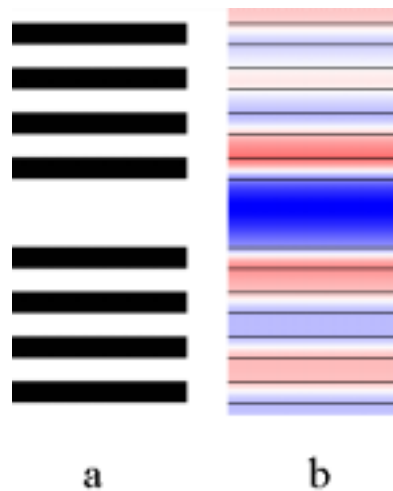
Figure 2.3.5 Defect (a) in a one-dimensional photonic crystal and the field pattern (b) of the corresponding defect mode.

Suppose that the defect consists of a single layer of the one-dimensional photonic crystal that has a different width than the rest. Such a system is shown in figure 2.3.5. In figure 2.3.5a, the structure and in figure 2.3.5b spatial pattern for the displacement field is shown. Note that displacement field is confined to defect introduced in the periodic structure. This mode is, that's why known as "defect mode". Thus, we no longer have a perfectly periodic lattice, but if we move many wavelengths away from the defect, the modes should behave as before.

Restricting our attention to on-axis propagation and let's consider a mode with a frequency ω in the photonic band gap. There are no extended modes with frequency ω inside the periodic lattice, and introducing the defect will not change that fact. The destruction of periodicity prevents us from describing the modes of the system with wave vector k, but we can still employ our knowledge of the band structure to determine whether a certain frequency will support extended states inside the rest of the crystal.

Defects may permit *localized* modes to exist, with frequencies inside photonic band gaps. If a mode has a frequency in the gap, then it must exponentially decay once it enters the crystal. The multilayer films on both sides of the defect behave like frequency-specific mirrors. If two such films are oriented parallel to one another, any-z propagating light trapped between them just bounce back and forth between these two mirrors. And because the distance between the

mirrors is of the order the light's wavelength, the modes are *quantized*. This situation bears strong resemblance to quantum mechanical problem of a particle in a box, or the electromagnetic problem of microwaves in a metallic cavity.

Consider the family of localized states generated by continously increasing the thickness of the defect layer. The bound mode associated with each member of this family will have a different frequency. As the thickness of the high-ε layer is increased, the frequency will decrease, because the field will be concentrated more and more in a high ε-region. Moreover, the rate of decay will be largest when the frequency is near the center of the gap, as shown in figure 2.3.4. States with frequencies in the center of the gap will be most strongly attached to the defect.

The *density of states* of a system is the number of allowed states per unit increase in ω. If a single state is introduced into the photonic band gap, then the density of states of the system is zero in the photonic band gap, except for a single peak associated with the defect.

2.4 Two-Dimensional Photonic Crystals

A two-dimensional photonic crystal is periodic along two of its axes and homogeneous along the third. A typical specimen, consisting of a square lattice of dielectric columns, is shown in figure 2.4.1. For certain values of the column spacing, this crystal can have a photonic band gap in the *xy*-plane. Inside this gap, no extended states are permitted, and incident light is reflected. This two-dimensional photonic crystal can reflect light incident from any direction in the plane.
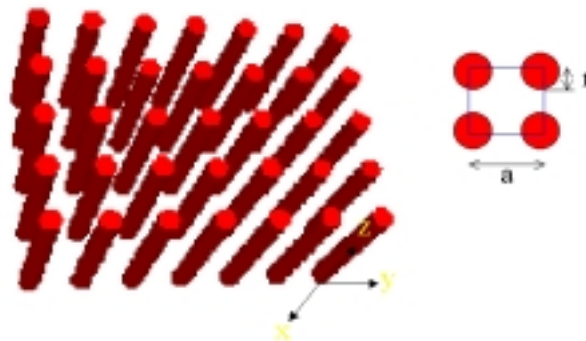
Figure 2.4.1 A representation of a two-dimensional photonic crystal.

As always, we can use the symmetries of the crystal to characterize its electromagnetic modes. Because the system is homogeneous in the z-direction, we know that the modes must be oscillatory in that direction, with no restrictions on the wave vector k_z. In addition, the system has discrete translational symmetry in the xy-plane. Specifically, $\varepsilon(\rho) = \varepsilon(\rho + R)$, as long as R is any linear combination of the primitive lattice vectors.
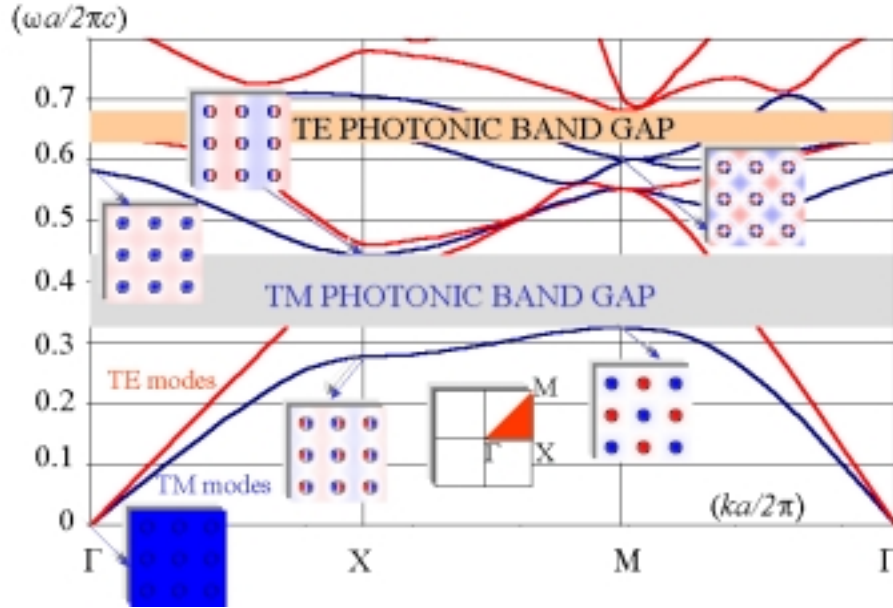
Figure 2.4.2 Photonic band structure of a square lattice of alumina rods.

Indexing the modes of the crystal by k_z, $k_{//}$, and n, they take the form

$$\mathbf{H}_{(n,\, k_z,\, k_{//})}(\mathbf{r}) = e^{i\mathbf{k}_{//}\cdot\rho}e^{ik_z z}\, \mathbf{u}_{(n,\, k_z,\, k_{//})}(\rho). \qquad 2.4.1$$

Here $\mathbf{u}(\rho)$ is a periodic function, $\mathbf{u}(\rho) = \mathbf{u}(\rho + R)$, for all lattice vectors R. The modes of this system look similar to those of the multilayer film. The key difference is that in the present case, $\mathbf{k}_{//}$ is restricted to the Brillouin zone and k_z is unrestricted. Also, $\mathbf{u}$ is now periodic in the plane.

If $k_z = 0$, so that light is propagating strictly in the xy-plane, then the system is invariant under reflections through the xy-plane. As discussed before, this symmetry allows us to classsify the modes by seperating them into two distinct polarizations. TE modes have $\mathbf{H}$ normal to the

plane and **E** in the plane. TM modes have just the reverse. The band structures for TE and TM modes can be completely different.

Consider light that propagates in the *xy*-plane of a square array of dielectric columns. The band structure for a crystal consisting of alumina ($\varepsilon = 8.9$) rods with *r/a* = 0.2 is plotted in figure 2.4.2. Irreducible Brilloun zone for the square lattice is also illustrated as an inset of figure 2.4.2. It is 1/8 of the first Brillouin zone.

The three special points Γ, X, and M correspond (respectively) to $\mathbf{k}_{//} = 0$, $\mathbf{k}_{//} = \pi/a\ \mathbf{x}$, and $\mathbf{k}_{//} = \pi/a\ \mathbf{x} + \pi/a\ \mathbf{y}$. What do the field profiles at these points look like?

The field patterns of the TM modes of the first and second band are shown in the insets of figure 2.4.2. For modes at the Γ-point, the fields are the same in each unit cell. The X-point is at the zone-edge, so the fields alternate in each unit cell along the direction of the wave vector k_x, forming wavefronts parallel to the *y*-direction. At M, the phases of the fields alternate in neighboring cells, forming a checkerboard pattern, like a plane wave propagating in the direction $\mathbf{x} + \mathbf{y}$.
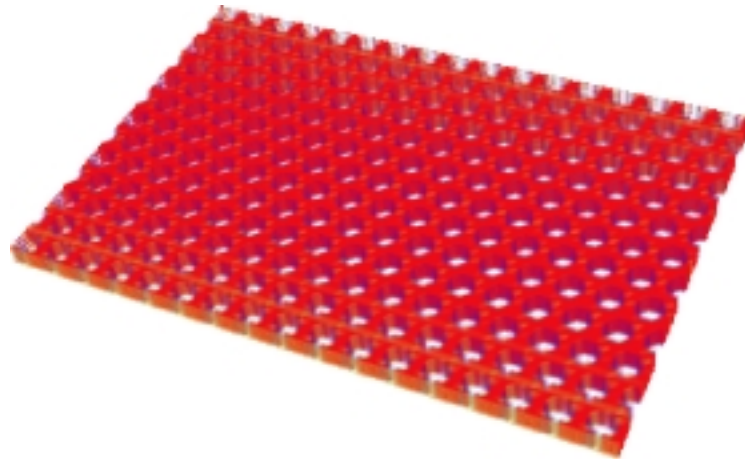
Figure 2.4.3 An illustration of the triangular lattice of air columns.

Field patterns in figure 2.4.2 confirms, according to electromagnetic variational theory, that the lowest frequencies settle in the highest dielectric constant regions, and the higher frequencies are allocated around the low-dielectric regions. This can be easily seen from the insets.

TM band gaps are favored in a lattice of isolated high-ε regions, and TE band gaps are favored in a connected lattice [2].

It seems impossible to arrange a photonic crystal with both isolated spots and connected regions of dielectric material. The answer is a sort of compromise: we can imagine crystals with high-ε regions that are both practically isolated and linked *and* linked by narrow veins.
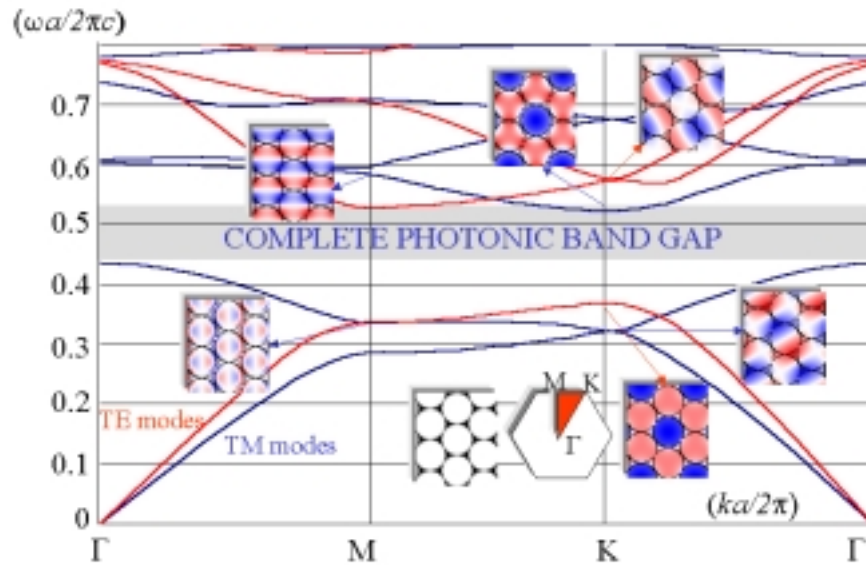
Figure 2.4.4 Photonic band structure of a triangular lattice of air columns.

An example of such a system is the triangular *lattice* of air columns, which is illustrated in figure 2.4.3. The band structure for a triangular lattice of air colums with a radius of 0.48a embedded in dielectric with a dielectric constant of 13 is sketched in figure 2.4.4. Note that a complete photonic band gap exists for this structure for both TE and TM polarizations. The irreducible Brilloun zone for triangular lattice is 1/12 of the first Brillouin zone and is shown as a red triangle in the inset. Spatial distribution of field pattern for corresponding points in the band structure are also illustrated in the insets. At the M point, only the displacement field for the TM modes below and above the gap is calculated. Note that lower frequency is concentrated around high-dielectric constant, again which confirms the variational principle. It is also clear from the picture above the gap at M point that the wavefronts are in the M direction. When looking at the K point, field distribution is given for both polarizations above and below the gap. These pictures also confirms the variational principle and the mode profiles have wavefronts propagating in the X direction. For TM modes displacement field,

and for TE modes magnetic field distribution is calculated. Thus, it must be noted that for TE modes, the displacement field is higher in the nodes, white regions.

The extent of a photonic band gap can be characterized by its frequency width $\Delta\omega$, but this is not a really useful measure. Remember that all the results are scalable, and the corresponding band gap in a crystal that is expanded by a factor of s woud have width $\Delta\omega/s$. A more useful characterisation, which is independent of the scale of the crystal, is the *gap-midgap ratio*, $\Delta\omega/\omega_0$.

By examining the field patterns for the square lattice of dielectric rods, we would find that there exists anology with the nomenclature of molecular orbits. The second and third bands are composed of "π-like" elements, with one nodal plane passing through each column. The bottom of the fourth band has "δ-like" elements with two nodal planes per column (see figure 2.4.5). Remember that additional nodal planes in the high-ε regions correspond to larger amplitudes in the low-ε regions, which increases the frequency.
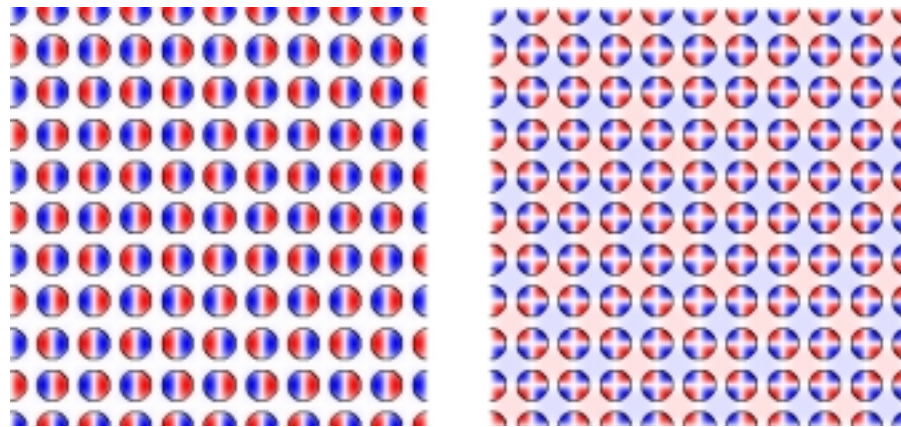
Figure 2.4.5 Field patterns for a square lattice of dielectric rods.

A defect in this array introduces a localized mode, as shown in figure 2.4.6. Experimentally this defect was introduced by replacing one of the columns with a column of a different radius. Computationally, the defect was introduced by varying the dielectric constant of a single column. In terms of the index of refraction $n = \sqrt{\varepsilon}$, the defect vaied from $\Delta n = n_{alumina} - n_{defect} = 0$ to $\Delta n = 2$ (one column completely gone).

Since the defect in the left panel of figure 2.4.6 is unchanged under 90° rotations, we can immediately predict te symmetry properties of the doubly degenerate modes that cross the gap for $0 < \Delta n < 0.8$. They must be a pair of modes that transform into each other under a 90° rotation, since that is the only doubly degenerate way to reproduce the symmetry of the surroundings.
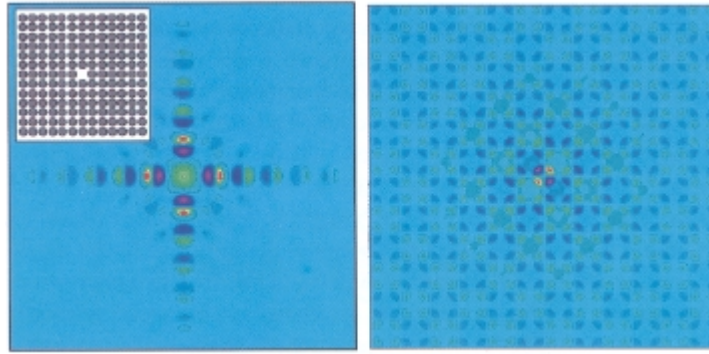
Figure 2.4.6 Defect in a square lattice of dielectric rods and corresponding defect modes [2].

Two surface terminations are depicted in the insets of figures 2.4.7 and 2.4.8, respectively. Because the translational symmetry in the *x*-direction is ruined, we can no longer describe the electromagnetic modes by a wave vector k_x. However, the system still has discrete translational symmetry in the *y*-direction, and continous translational symmetry in the *z*-direction. We can still classify the modes of the surfece Brillouin zone with wave vectors k_y and k_z, which are bounded by $-\pi/a < k_y \leq \pi/a$ and $-\infty < k_z < \infty$. The following discussion is limited to in-plane propagation, for which $k_z = 0$.

To determine where the *surface modes* exist, we pick a specific (ω_0, k_y) and ask if there is any k_x which will put that mode on a band. That is, by a suitable choice of k_x, can we arrange for some band *n* that $\omega_0 = \omega_n(k_x, k_y)$? If we can, then there is at least one extended state in the crystal with that combination (ω_0, k_y). If we tried to set up a surface modes with those parameters, it would not be localized; it would leak into the crystal.

This process of searching all possible k_x for each k_y is called "projecting the band structure of the infinite crystal into the surface Brillouin zone." We take all of the information from the full crystal band structure, and extract the information relevant for the surface. A true,

localized, surface mode must be evanescent both inside the crystal and outside, in the air region, so we must project the band structure of both the photonic crystal and the air region.
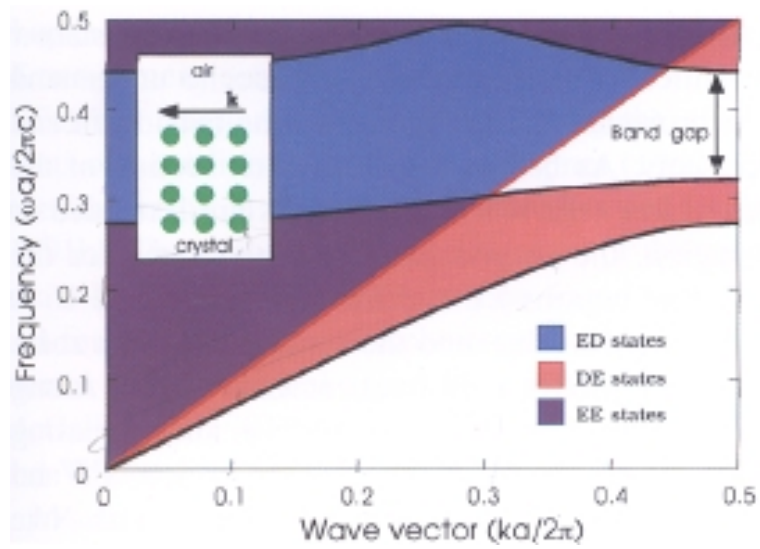
Figure 2.4.7 The surface band structure of the constant-*x* surface of a square lattice of alumina rods in air with a regular termination.
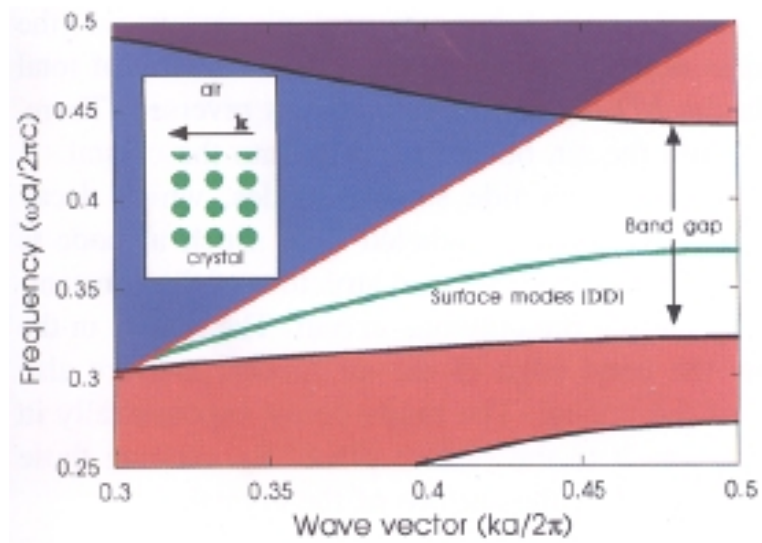
Figure 2.4.8 The surface band structure of the constant-*x* surface of a square lattice of alumina rods in air with an irregular termination.

Figure 2.4.7 shows the projected band structure of the constant-*x* surface of square lattice of dielectric rods. In order to understand it, the projected band structures of the outside air and photonic ctystals are considered seperately. As before,each section of the plot is labeled with

two letters. The union of regions *EE* and *ED* shown in figure 2.4.7 is the projection of the free light modes at all frequencies $\omega \geq c|k_y|$. Along the line $\omega = ck_y$, the light travels parallel to the surface, and increasing ω corresponds to increasing k_x. Similarly, the union of regions *EE* and *DE* represents the projected band structure of the photonic crystal.

Now, we can understand the three types of surface states of the projected surface Brillouin zone: light that is transmitted (*EE*), light that is internally reflected (*DE*), and light that is externally reflected (*ED*).

Finally, there might exist surface modes, which decay away from *both* sides of the surface (labeled *DD*). Such a mode is displayed in figure 2.4.8, which shows the band structure of the constant-*x* surface terminated by cutting columns in half.

2.5 Three-Dimensional Photonic Crystals

There are an infinite number of possible geometries for a three-dimensional photonic crystal, but we are particularly interested in those geometries that promote the existence of photonic band gaps. Some examples are given in figures 2.5.1, 2, 3, and 4. 3D photonic crystals shown in figures 2.5.1 and 2 are fabricated at MIT by the Joannopoulos' group. Figures 2.5.3 and 4 show 3D photonic crystals composed of bars and spirals, respectively.
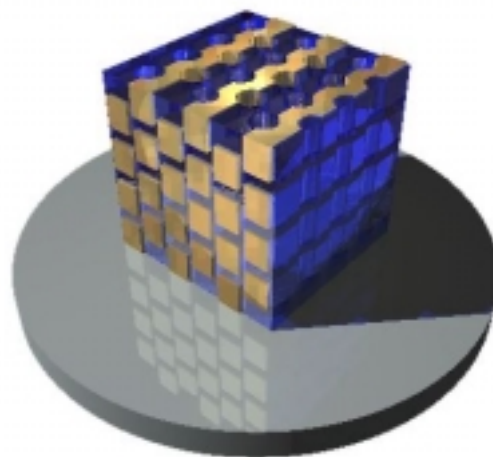
Figure 2.5.1 A 3D photonic crystal fabricated at MIT [3].

3D photonic crystals can be formed by mainly two methods. The first type is created by taking a three-dimensional lattice and placing a sphere at each lattice point. We can completely characterize crystals of this type by the lattice vectors, the dielectric constants of the spheres and the embedding material, and the radius of the spheres. We can also, reverse the dielectric constants, and place air bubbles in a dielectric material.

The second type results from taking a lattice and connecting the lattice points with cylindirical columns. This type of crystal can be characterized by the dielectric constants of the different regions, the pattern and angles of drilling, and the radius of the holes.
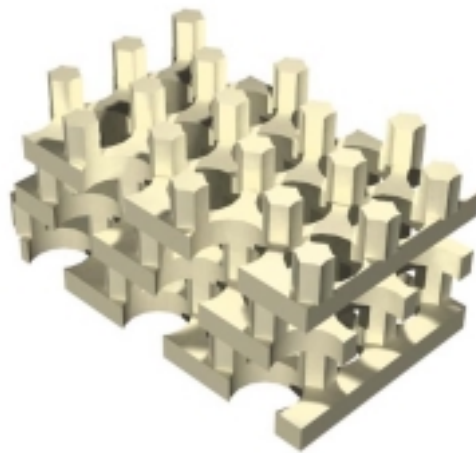
Figure 2.5.2 Another sample of a 3D photonic crystal fabricated at MIT [3].
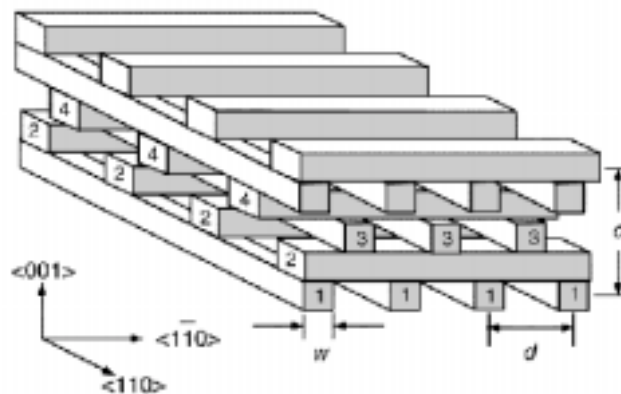
Figure 2.5.3 A 3D photonic crystal with face centered tetragonal symmetry [4].

2.6 Comparison of the Electronic Band Gap (EBG) with the Photonic Band Gap (PBG)

1) The "master equation" that determines the normal modes of the system is the Schrodinger equation for the EBG and the Maxwell equations for the PBG.

2) The periodicity of the system enter as the potential: V($\mathbf{r}$) = V($\mathbf{r}$+$\mathbf{R}$), for all lattice vectors $\mathbf{R}$ for the EBG, and the dielectric: ε($\mathbf{r}$) = ε($\mathbf{r}$+$\mathbf{R}$) in the PBG case.

3) In the EBG case, there is an electron-electron repulsive interaction that makes large scale computation difficult. However, in the PBG case, in the linear regime, light modes can pass right through one another undisturbed, and can be calculated independently.

4) In the EBG case, eigenstates with different energies are orthogonal, they have real eigenvalues, and can be found with a variational principle. In the PBG case, modes with different frequencies are orthogonal, they have real positive eigenvalues, and can also be found with a variational principle.
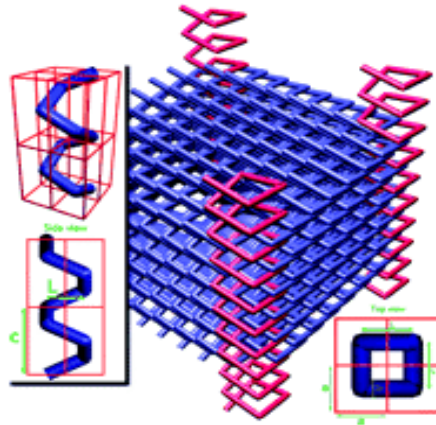
Figure 2.5.4 A 3D photonic crystal composed of the periodic array of spirals [5].

5) In the EBG case, master equation relies on the Hamiltonian, *H*, which is a linear and Hermitian operator. In the PBG case, it is the Maxwell operator Θ, on which the master equation relies on and it is also linear and Hermitian operator.

6) In the EBG case, the wave function concentrates in regions of low potential, while remaining orthogonal to lower states. In the PBG case, the fields concentrate their electrical energy in high-ε regions, while remaining orthogonal to lower modes.

7) The physical energy of the system in the EBG case is the eigenvalue *E* of the Hamiltonian; and the electromagnetic energy in the PBG case.

8) In both cases we distinguish the normal modes by how they transform under a symmetry operation *A*.

9) The discrete translational symmetry of a crystal allow us to write wave function in Bloch form in the EBG case; and to write the harmonic modes, $\mathbf{H_k(r)} = \mathbf{u_k(r)}e^{i\mathbf{k}\cdot\mathbf{r}}$, in Bloch form in the PBG case.

10) In the EBG case, the physical origin of the band structure is the coherent scattering of electrons from the different potential regions; and the coherent scattering of electromagnetic fields at the interfaces between different dielectric regions, in the PBG case. This analogy is depicted in figure 2.6.1.

11) In the EBG case, no propagating electrons in that energy range are allowed to exist, regardless of wave vector. In the PBG case, however, no extended modes in that frequency range are allowed to exist, regardless of wave vector.
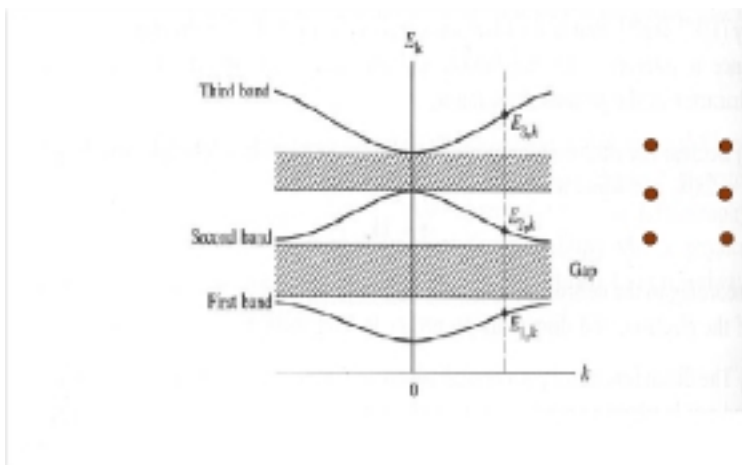
Figure 2.6.1 An analogy between photonic and electronic band gap [6].

12) In the EBG case, the band above the gap is the *conduction band*; the band below the gap is the *valence band*. In the PBG case, they are the *air band* and *dielectric band*, respectively.

13) In the EBG case, defects can be introduced by adding foreign atoms to the crystal, which breaks the translational symmetry of the atomic potential. In the PBG case, they are introduced by changing the dielectric constant of certain regions, which breaks the translational symmetry of $\varepsilon(\mathbf{r})$.

14) The result of introducing a defect is an allowed state in a band gap, thereby permitting a localized electron state around the defect in the EBG case. In the PBG case, this might create an allowed state in a band gap, thereby permitting a localized mode around the defect.

15) In the EBG case, donor atoms pull states from the conduction band into the gap; acceptor atoms pull states from the valence band into the gap. In the PBG case, dielectric defects pull states from the air band into the gap; air defects pull states from the dielectric band into the gap.

16) Study of the physics of the EBG can lead to tailor the *electronic* properties of materials to our needs and the study of the physics of the PBG can lead to tailor the *optical* properties of materials to our needs.

2.7 Some Examples of Photonic Crystal Applications

Long ago, engineers solved the problem of controlling light propagation in the microwave regime by using metallic components to guide, reflect, and trap light. These components rely on a rather complicated electronic property that may depend strongly on frequency. Unfortunately, for light of higher frequency, metallic components suffer from high dissipative losses.

The reflectivity of photonic crystals derives from their geometry and periodicity, not a complicated atomic-scale property. The only demand we make on our materials is that for the frequency range of interest (which is often a narrow band), they should be essentially lossless. Such materials are widely available all the way from the ultraviolet regime to microwave. The photonic properties scale easily with frequency and ε, so devices made at one scale are sure to work at other scales.

Since the heart of many devices is reflectivity, let's look at how to design a two-dimensional crystal that reflects all in-plane light within some specified frequency band, without appreciable absorption. Once finished, we could use this crystal in a band-stop filter. Or, since the band structures of two-dimensional photonic crystals are different for TE and TM light, we could employ it as a polarizer. Or we can use it to make resonant cavities and dielectric waveguides.

For concreteness, let's assume elements for a particular wavelength of light: $\lambda = 1.5$ μm, the wavelength of light which is often used in telecommunications. Suppose we construct the crystal from GaAs, a material widely used in optoelectronics. For light with a wavelength

between λ = 1.0 μm and λ = 10.0 μm has a dielectric constant of 11.4. Can we design a photonic crystal to meet these specifications?

In order to make a reflecting structure, we need to choose a crystal geometry that provides a photonic band gap. We should also choose a geometry that is relatively easy to fabricate at micron-level dimensions. After consulting the gap map in figure 2.7.1, we notice a particualry simple geometry with those characteristics: the triangular lattice of air columns. It has band gaps for both TE and TM modes, it has an overlapping band gap for both polarizations, and we can make it simply etching holes into a GaAs sheet.

If we wanted to make a polarization-sensitive device, we would choose a band gap for either TE or TM modes alone. Here, let's choose the overlapping region on the gap map, in which all in-plane light is reflected, regardless of polarization. That region's thickest extent occurs when $r/a = 0.45$, and the gap is centered around $\omega a/2\pi c = 0.5$. We have chosen $\lambda = 2\pi c/\omega = 1.5$ μm, so we need

$$\omega a/2\pi c = a/\lambda = a/(1.5 \text{ μm}) = 0.5 \qquad a = 0.75 \text{ μm}. \qquad 2.7.1$$

The condition that the wavelength is 1.5 μm has provided a, and now we use the condition that there is a complete band gap to determine r. Setting $r/a = 0.45$, we find $r = 0.34$ μm. Our structure is now determined completely: we will use a GaAs substrate in which air holes of radius 0.34 μm have been etched in a triangular pattern, with lattice constant of 0.75 μm.

As we can see from figure 2.7.1, the extent of the band gap is from $\omega a/2\pi c = a/\lambda = 0.45$ to $\omega a/2\pi c = 0.55$. The gap-midgap ratio is $0.1/0.5 = 20\%$. The frequency band corresponds to a wavelength band from λ = 0.73 μm to λ = 1.7 μm. This region is adequately covers the frequncy range of interest.

What else can we do? Defects admit the existence of localized modes within a very narrow frequency band. For example, if we place a defect in our triangular lattice of air columns, and we excite a mode with a frequency within the band gap, the light will have nowhere to go. It will be trapped by perfectly reflecting walls. Of course, our structure will only confine light in the plane of periodicity. To prevent it from escaping in the third direction, another method

would be needed -one might sandwich the triangular lattice between two metallic plates, or two dielectric slabs (counting on total internal reflection). Alternatively, one could use a fully three-dimensional pahotonic crystal. But for pedagogical purposes, we will remain focused on the two-dimensional case.

Why would we want to create a defect mode? One obvious answer is to serve as a resonant cavity. Such cavities are crucial components of laser systems. A defect mode in a photonic crystal would serve as an effective resonant cavity, since it would only trap light in a very narrow frequency band and would hardly suffer any losses. The "quality factor" Q, measure of how many oscillations take place in a cavity before damping eventually dissipates away the original excitation, would be high.
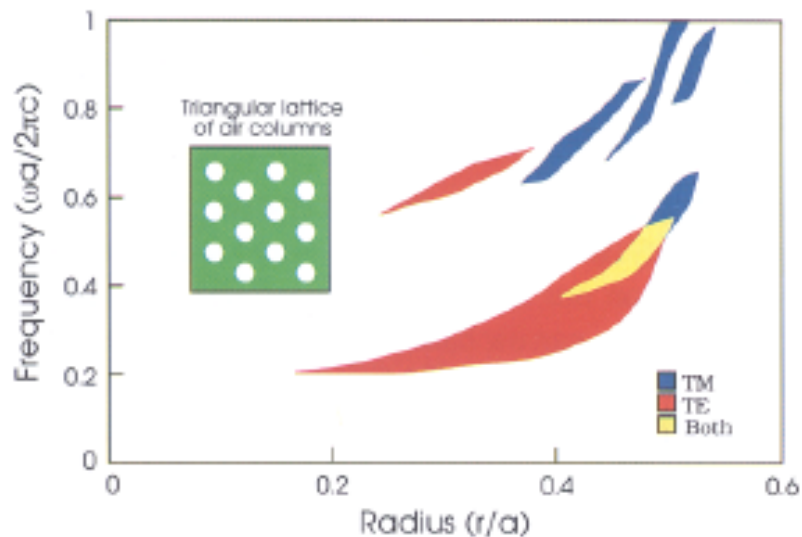
Figure 2.7.1 Gap map for a triangular lattice of air colums in GaAs [2].

In fact, a resonant cavity would be useful whenever one would like to control radiation within a narrow frequency range. For example, all atomic transitions from one energy level to another are acompanied by the emission or absorption of photons, with energies corresponding to the difference in those energy levels. One can imagine selecting and suppressing various atomic transitions by having them take place in appropriate photonic crystals.

The important questions to address when designing a defect mode are how the defect shall be introduced into the structure, and which frequencies it will support as localized modes. First,

one obvious way to introduce a defect is to allow one of the columns of the triangular lattice to grow or shrink in radius.
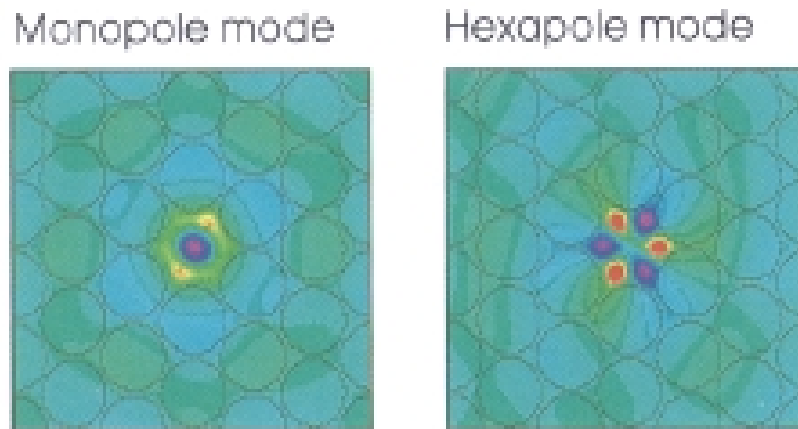
Figure 2.7.2 Magnetic field patterns of defect modes in a triangular lattice missing a single air column [2].

For concreteness, let's choose the case $r_d = 0$, so that the triangular lattice is missing a single air column. We can use our structure as a resonant cavity for modes of frequency $\omega a/2\pi c =$ 0.31, 0.39, 0.42, and 0.46. In this case the defect resembles a cavity with perfectly reflecting walls, and the mode frequencies of such a cavity can be estimated just like they can for metallic cavities -by requiring that the field go to zero at the boundaries, so that either half a wavelength , a full wavelength, a wavelength and a half, etc. fits perfectly in the cavity. The magnetic field patterns for the defect modes of the structure are shown in figure 2.7.2.

We can use point defects in photonic crystals to trap light. By using line defects, we can also *guide* light from one location to another. The basic idea is to carve a waveguide otherwise-perfect photonic crystal. Light that propagates in the waveguide with a frequency within the band gap of the crystal is confined to, and can be directed along, the waveguide. I will not explain how to design waveguide here, I will defer to chapter 3, where I will describe the waveguide we used in the project.

Microwaves are already commonly guided by metallic guides and coaxial cables, but we have already discussed the limitations of these methods. Visible light can be guided with fiber-optic cables, which rely on total internal reflection. However, if a fiber-optic cable takes a tight curve, light escapes at the corners and is lost. Photonic crystals, since they do not rely on total internal reflection, continue to confine light even around tight corners.

For these reasons, photonic crystal waveguides can find use whenever a monochromatic light beam needs to be guided from one location to another. These situations are becoming increasingly common in modern technology. In an optoelectronic circuit, light is guided from one end of a microchip to another. In a fiber-optic network, like those used in telecommunications, light is guided from one end of the country to another.

Once light is induced to travel along the waveguide it really has nowhere else to go. Since the frequency of the guided mode lies within the photonic band gap, the mode is forbidden to escape into the crystal. Regardless of the shape of the waveguide, light is forced to bounce around inside it. The primary source of loss can only be reflection back out the waveguide entrance. This suggests that we may use a photonic crystal to guide light around tight corners. Returning to our square lattice of GaAs rods in air, we can carve out a waveguide with a sharp 90 degree band as shown in figure 2.7.3. Here is plotted the displacement field of a propagating TM mode as it travels around the corner. Even though the radius of curvature of the bend is less than the wavelength of the light, very nearly all the light that goes in one end comes out the other!
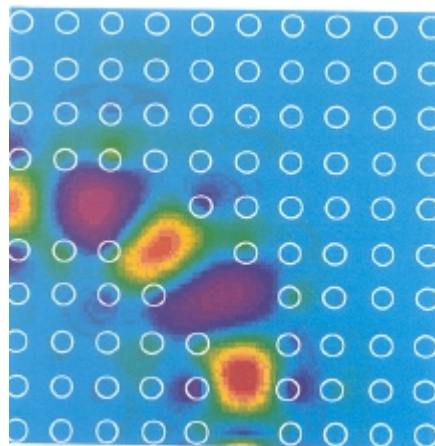
Figure 2.7.3 The displacement field of a TM mode traveling around a sharp bend in a waveguide carved out of a square lattice of dielectric rods [2].

2.8 Trapping and Emission of Photons by a Single Defect in a Photonic Bandgap Structure
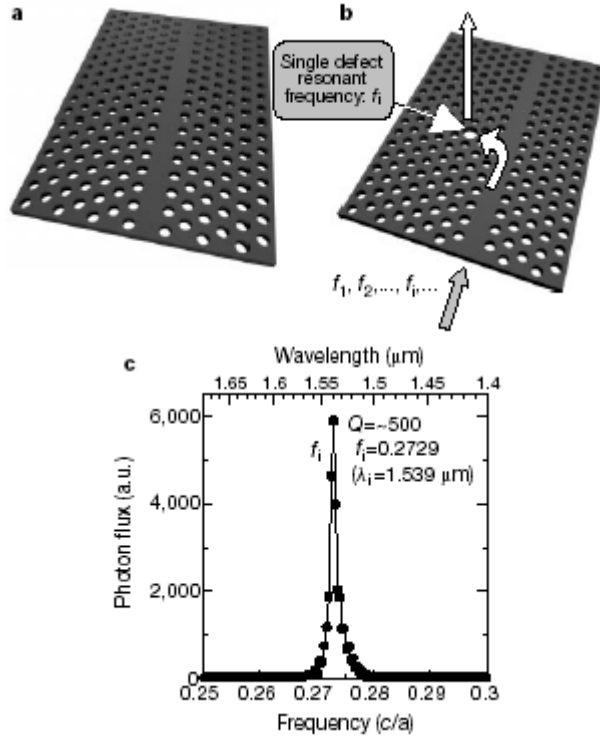
Figure 2.8.1 Trapping and emission of photons by a single defect in a photonic band gap.

I have got much enlightenment from the paper of Noda et al [1], Nature (2000). In this work a two-dimensional photonic crystal structure with a triangular lattice of air holes is considered. The in-plane confinement of light is accomplished by the photonic bandgap (PBG) effect and vertical confinement is achieved by the large refractive index contrast with the cladding air. The structure is designed to have a band-gap for the TE-like modes. The radius of each hole and the slab thickness is chosen to be $0.29a$ and $0.6a$, respectively, where a is the lattice constant. A linear defect is introduced in the structure as shown in fig. 2.8.1a. Using 3D FDTD method, it is confirmed that the waveguide has a lossless transmission in the range $(0.27\text{-}0.28)(c/a)$, where c is the lightspeed in the vacuum. Then an isolated point defect, with a radius and distance to waveguide $0.56a$ and $3\sqrt{3}/2a$, respectively, is introduced in the vicinity of the waveguide as shown in fig. 2.8.1b. It is shown that the defect acts as an optical resonator with a normalized frequency of $0.2729(c/a)$ and a quality factor of around 500, respectively. Taking $a = 0.42$ μm, this frequency corresponds to 1.539 μm. The quality factor for the resonator can be determined by two components. Q_{in} is for in-plane direction and primarily determined by the distance between the defect and the waveguide. Q_v is for the vertical direction and depends on the effective refractive index contrast between the defect and the cladding air.

The flux of photons which are trapped from the waveguide and emitted to free sapce by the single defect was calculated by the 3D FDTD method and the result is shown in figure 2.8.1c. In this work Q_{in} and Q_v are almost equal, which lead to half of the photons from the waveguide are emitted from the defect to free space.
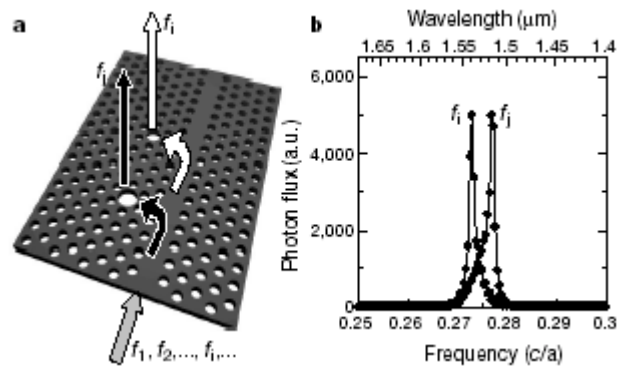
Figure 2.8.2 Trapping and emission of photons by two isolated defects.

In this paper it is demonstrated that it is possible to filter out very narrow frequency band from a certain range of frequency. For example, figure 2.8.2a shows the trapping and emission of two different frequencies by the isolated point defects. Second defect introduced into the structure has a radius of $0.58a$ with a resonant frequency corresponding to 1.517 μm. In figure 2.8.2b is shown the calculated photon flux emitted by two defects. The mutual interaction of the defects are not considered in the calculation.
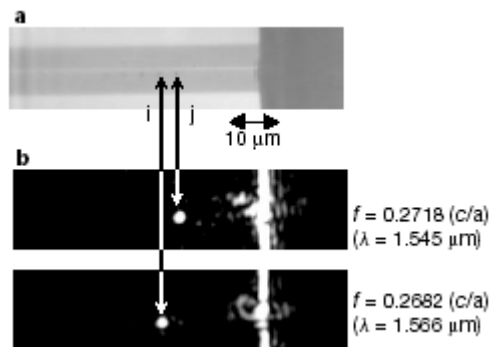
Figure 2.8.3 Experimental results of trapping and emission of photons by defects.

Experimental results are shown in figures 2.8.3 and 4. Figure 2.8.3a shows the top view of the structure observed by optical microscope. The light is injected to the waveguide from the right edge of the slab. Figure 2.8.3b shows the observation by an infrared camera. Note that two resonant frequencies are clearly seen in the figure and figure 2.8.4 shows the experimental result for the emitted photon flux from a single defect which fits quite well with the theoretical calculations.
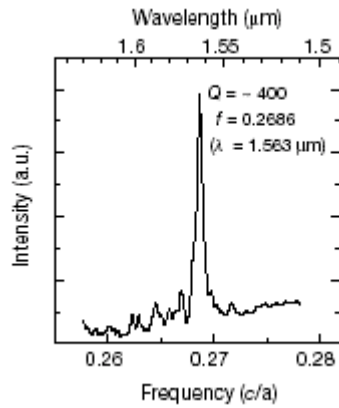
Figure 2.8.4 Emitted photon flux from a single defect as a function of normalized frequency.

3. A TWO-DIMENSIONAL PHOTONIC CRYSTAL FOR SURFACE TEMPERATURE MAPPING

3.1 Introduction

In the last century, the control over electrical properties of materials led to transistor revolution in electronics. Now, in this century, photonic crystals inspired great interest to control the flow of light. Photonic band gap materials seem to be more promising as a base medium both for future laser based photonic integrated circuits and maybe later on for advanced quantum network technologies as well [2,7,8].

The capabilities of perfect periodic arrangements of dielectric materials (i.e., photonic crystals) to control the propagation of electromagnetic waves have been well studied since the primary predictions of Yablonovitch and Gmitter [9-15]. In analogous to crystalline solids with a periodic potential for electronic wavefunctions, photonic dispersions are strongly perturbed by the spatial periodicity of dielectric function in the photonic lattice. The strongest effect is experienced at the high symmetry points of the photonic Brillouin zone where electromagnetic gaps with no propagating states exist. The size of these gaps depends on the refractive index contrast, the filling fractions of the dielectric media and some other parameters of the lattice too [16]. In contrast to the conventional waveguides, the mechanism of confinement within the PBG waveguide is not due to the total internal reflection, but could

be explained by an optical quantum well, which does not allow the modes within the surrounding region of the waveguide. This is the reason why light becomes confined to the modes within the PBG [17]. In addition, for example, a line-defect can be introduced into the PBG material by adding, removing or distorting material in the crystal. These defects break the above symmetry and may give rise to the otherwise not allowed defect states within the PBG region of the photonic crystal. It is well known that introducing defects in electronic band gap materials allows the electronic wavefunctions to have energy in the electronic band gap. Thus, the electronic wavefunction is localized around the impurity. Similarly, introducing defects in the PBG materials, one can localize and control the properties of electromagnetic wavefunctions, thus making these materials ever more useful. Defect states appear as spikes when viewing the transmission response in the PBG region [9,18]. One can also use point defects in the photonic crystals to trap light [1,2]. Therefore, the electromagnetic wave with a frequency in the gap can be guided along the line defect from one location to another without appreciable losses [2,19], and the application in this paper is mostly based on this peculiar property of the photonic crystal waveguides.
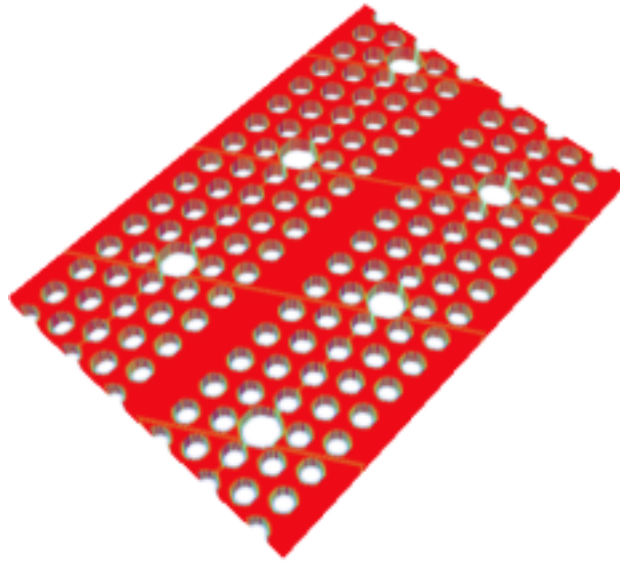
Figure 3.2.1 2D PBG slab consisting a triangular array of air holes etched into the substrate with one straight waveguide and isolated point defects.

Many studies have been carried out concerning guided modes in the 2D PBG materials [10,11,16,19-21]. However, very few studies can be found in the literature concerning the sensor applications. In this paper, we propose a photonic crystal structure, as an infrared (IR)

detector for temperature reading of the objects, that makes use of the effect of a 2D PBG to confine light in the in-plane direction for TE-like modes with large refractive index contrast to confine light in the vertical direction. The photonic device consists of triangular array of air holes etched into GaAs with linear and various isolated point defects. The operational principle of the photonic band gap device is based on guiding wavelengths around 1.55 μm and filtering out some specifically selected multiple optical frequencies through the isolated point defects. Having processed the intensities of the selected optical frequencies (or wavelengths), using the blackbody radiation characteristics of the object in concern and the transmission properties of the device, the surface temperature of the target can be obtained. The proposed photonic device has also potential for multiplexing and, in contrast to conventional blackbody radiation detection systems, it does not require the detailed knowledge of emissivity, transmission loss and distance-to-target-size ratio.

3.2 The Photonic Crystal Structure and the Working Principle

Figure 3.2.2 Working principle of the photonic crystal device.
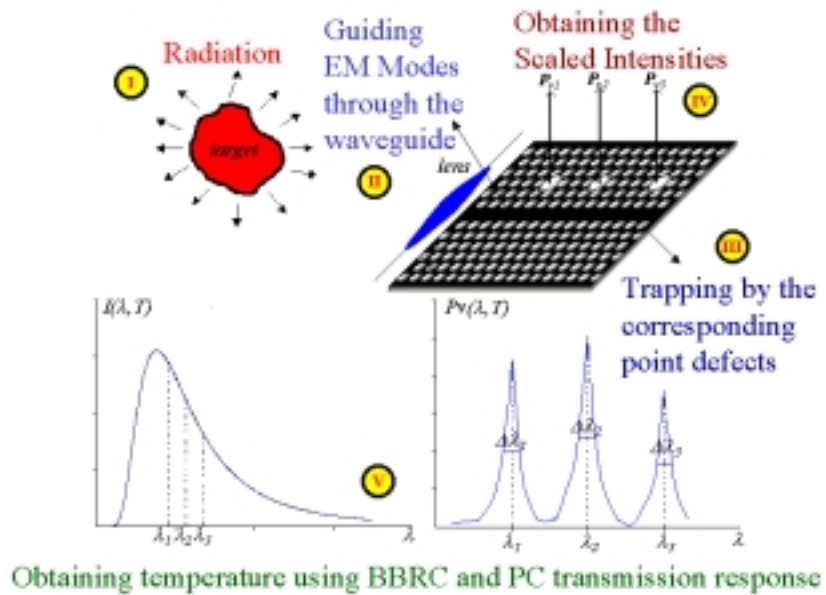
The photonic crystal structure, considered in this work is a 2D PBG slab which consists of triangular array of air holes etched into the substrate with one straight waveguide and isolated point defects, shown in figure 3.2.1. Because it is lossless through the spectral region chosen, optical properties of GaAs are used in the device simulation. The transduction mechanism of

the PBG device is based on guiding and filtering out of specifically tuned three optical wavelengths (λ_1, λ_2, and λ_3) transmitted through the waveguide, as shown in figure 3.2.2. Figure 3.2.3 is another description of working principle. Basically, the light, which is filtered out by the device, is sent to a processor unit there, which the surface temperature mapping of the objects is obtained.
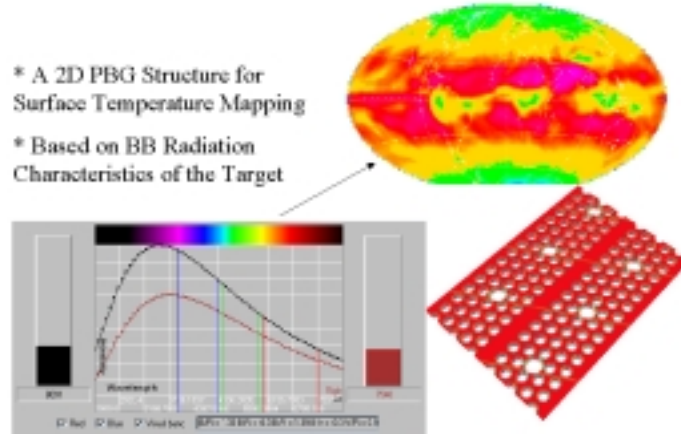
Figure 3.2.3 Another description of operation.

Let us assume that the object is at temperature *T*, and is emitting optical radiation according to the blackbody radiation characteristic curve (see Fig. 3.2.4). In figure 3.2.4, it is depicted how the optical power is reduced on its way to the sensor unit of the device. Note that the reduced intensity is the output and the temperature is obtained by the processing of output together with the characteristics of the device. The radiated optical power from the object per meter square per wavelength, ie, W/m²μm, at λ is given by well-known Planck's formula as

$$I(\lambda,T) = \frac{2\pi hc^2}{\lambda^5} \frac{1}{e^{hc/\lambda kT} - 1} \qquad 3.2.1$$

where, *h, c, λ, k, T* stand for the Planck's constant, speed of light in vacuum, radiation wavelength, the Boltzmann constant, and the temperature, respectively. Figure 3.2.2 depicts a plot of eq.3.2.1 at a constant temperature *T* and covers a very broad wavelength range. As shown in Figure 3.2.2, if we place our PBG device in front of the radiating object, we should be able to filter out the wavelengths that are indicated on the object's blackbody radiation curve. The relation between the measured optical power, $P_{vi}(\lambda_i,T)$, which corresponds to

such resonant wavelengths for the isolated point defects from the PBG structure, and those are indicated on the blackbody characteristic curve in figure 3.2.2 (see also fig. 3.2.4) can be defined as

$$P_{vi}(\lambda_i, T) = S\gamma_i \int_{\lambda_i - \Delta\lambda_i/2}^{\lambda_i + \Delta\lambda_i/2} I(\lambda_i, T)d\lambda_i \qquad \text{3.2.2}$$

where,

$$P_{vi}(\lambda_i, T) \equiv \int_{\lambda_i - \frac{\Delta\lambda_i}{2}}^{\lambda_i} \frac{dP_v}{d\lambda}d\lambda - \int_{\lambda_i}^{\lambda_i + \frac{\Delta\lambda_i}{2}} \frac{dP_v}{d\lambda}d\lambda \qquad \text{3.2.3}$$

Here, S is called the scaling factor, which is explained below, and γ_i is the output efficiency for the defect in concern. The integral limits are taken over the full width at half maximum (i.e., $\Delta\lambda$) for the photon flux trapped from the waveguide and emitted to free space from a single defect of resonant wavelength λ_i, as seen in figure 3.2.2. By making use of Eq.2, the temperature of the object can be obtained by taking the ratio of optical power for any two defects. Let us consider the power ratio for any defect pairs, say, i and j; thus

$$\frac{P_{vi}(\lambda_i, T)}{P_{vj}(\lambda_j, T)} = \frac{\gamma_i}{\gamma_j} \frac{\int I(\lambda_i, T)d\lambda_i}{\int I(\lambda_j, T)d\lambda_j} \qquad \text{3.2.4}$$

For a numerical solution of eq.3.2.4, we need to express it in a discrete form; that is,

$$\frac{\sum_{k}^{n}\left(\frac{\delta P_{vik}}{\delta\lambda_{ik}}\right)\delta\lambda_{ik}}{\sum_{l}^{m}\left(\frac{\delta P_{vjl}}{\delta\lambda_{jl}}\right)\delta\lambda_{jl}} = \frac{\gamma_i}{\gamma_j} \frac{\sum_{k}^{n}\left[1/(\lambda_{ik}^5 \, exp(hc/\lambda_{ik}kT)-1)\right]\delta\lambda_i}{\sum_{l}^{m}\left[1/(\lambda_{jl}^5 \, exp(hc/\lambda_{jl}kT)-1)\right]\delta\lambda_j} \qquad \text{3.2.5}$$

In eq.3.2.5, the boundary conditions determine the corresponding range of wavelengths to be discretized in the Planck's formula, where, $\lambda_{ik} \equiv \lambda_i - \Delta\lambda_i/2 + (k-1/2)\delta\lambda_i$; and, $\lambda_{jl} \equiv \lambda_j - \Delta\lambda_j/2 + (l-1/2)\delta\lambda_j$. For example, $(n-1)\delta\lambda_i = \Delta\lambda_i$.
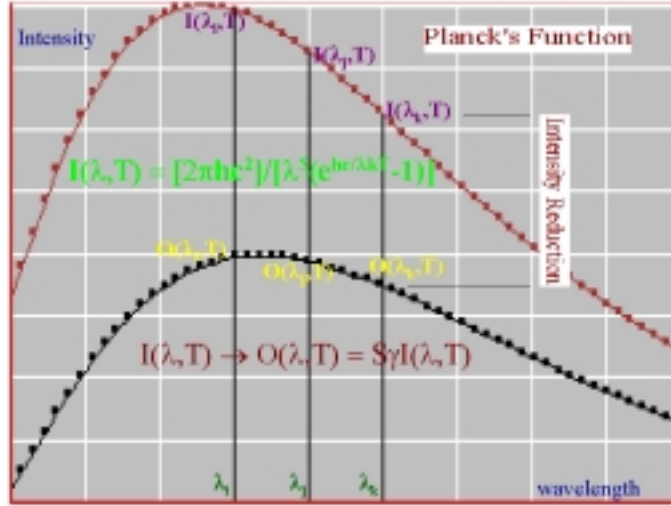
Figure 3.2.4 Comparison of output and input intensity on the blackbody characteristics.

To evaluate the temperature, first we express eq.3.2.5 as

$$\frac{\sum_{k}^{n} \delta P_{vik}}{\sum_{l}^{m} \delta P_{vjl}} - \frac{\gamma_i}{\gamma_j} \frac{\sum_{k}[1/\exp(hc/\lambda_k T - 1)]\delta\lambda_i}{\sum_{l}[1/\exp(hc/\lambda_l T - 1)]\delta\lambda_j} \equiv f(T) \qquad 3.2.6$$

Equation 3.2.6 tells us that only a correct value of temperature T' will satisfy the right-hand side of the equality to be zero. That is,

$$\lim_{T \to T'} f(T) = 0 \qquad 3.2.7$$

As can be seen in eq. 3.2.2 that the output radiation, which is emitted from the PBG structure, has a constant scaling factor S throughout the spectral region chosen, which can be represented as $S = X\Theta\prod R$; where X is the coupling of the photons to the photonic crystal structure from outside of the slab; Θ is the transmission response of the micromachined lens to be used as collecting optics; Π is a scaling factor due to the TE polarizer; and R is the power loss components including the emissivity and target-to-detector distance. The relation between γ_i and the quality factor, Q, is as follows: The quality factor of the optical resonators can be represented as $1/Q = 1/Q_{in} + 1/Q_v$, where Q_{in} and Q_v are the quality factors for in-plane and vertical directions, respectively. Q_{in} is primarily related to the defect-to-waveguide-

distance and can be expressed as $Q_{in} = \omega_0 U(t)/P_{in}(t)$; and $Q_v = \omega_0 U(t)/P_v(t)$, which is determined by the effective refractive index contrast between the defect and the cladding air. In these equations, $\omega_0 = 2\pi c/\lambda$, $U(t)$, $P_{in}(t)$, $P_v(t)$ denote resonant frequency, total energy in the defect at time t, total output power from the defect for in-plane and vertical directions at time t, respectively. On the other hand, when the values of Q_{in} and Q_v are equal, we get $P_{in}(t) = P_v(t)$, which means that half of the photon flux flowing through the waveguide can be trapped and emitted to the free space. When a large mismatch between the values of Q_{in} and Q_v is present, the emitted photon flux becomes smaller. In the case of $Q_{in} > Q_v$, although the power of vertical direction is larger than that of the in-plane direction, power emitted to the free space is less. This is because of the increase in the transmitted power without coupling to the defect. For the case $Q_{in} < Q_v$, however, the reason for the less power emitted to the free space is the higher reflection from the defect.

This situation resembles the electronic analogy of the phenomena, where the power transfer from the circuit to the load becomes maximum when the output impedance of the electronic circuit is equal to the impedance of the load [1,26]. Therefore an additional scaling factor, γ_i, is needed, where it is 0.5 at the maximum power transfer and smaller when a mismatch exists and could be found by 3D FDTD method. After all the effective scaling factors manifested themselves, the reduced intensity corresponding to each defect filtered out of the device is indicated, and the temperature of the object is obtained from these intensities using eq.3.2.6. For N defect points, a matrix can suitably represent the relationship between $P_{vi}(\lambda_i, T)$ and $I(\lambda_i, T)$.

In light of this promising analysis, it is clear that the photonic crystal slab considered has potential for the scaling property, which the transduction mechanism of the proposed device is based on. Since the size of the defects are of the order of one wavelength and photons are emitted in a direction normal to the surface, the structure could be applied to a very compact wavelength-monitoring device [19] including the surface temperature reading of micron-sized objects, if integrated with an appropriate micromachined lens of a certain transmission response.

3.3 Design and Simulation of the PBG Structure

The hole radius of the PBG structure shown in figure 3.2.1 was chosen to be $r = 0.3a$, where a is the lattice constant and is tuned to be 0.382 μm. The dielectric constant of GaAs is assumed to be $\varepsilon_r = 11.4$. The desired photonic crystal was designed to have a bandgap in 0.213-0.280 (c/a) for transverse-electric (TE) like modes, using MPB [27,28]. The band gap structure is shown in figure 3.3.1. The magnetic field spatial distribution for the points, corresponding to the modes just below and above the gap, are calculated at the high symmetry fields. Keeping in mind that the displacement field is maximum at the nodes in the field patterns shown in figure 3.3.1, we can assure the electromagnetic variational principle.
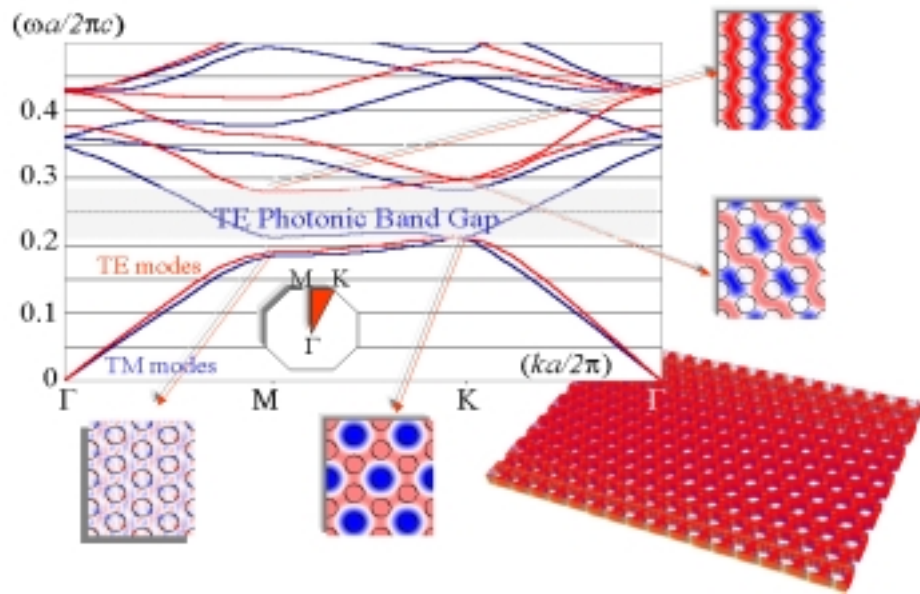
Figure 3.3.1 Photonic band structure for the designed device.

Suppose we want to construct a TE waveguide for 1.55 μm light. As before, we begin by consulting a gap map. For a triangular lattice of air holes in GaAs substrate we find that a TE gap occurs for $r = 0.3a$. This corresponds to a mid-gap frequency near $\omega a/2\pi c = a/\lambda = 0.2465$, and since $\lambda = 1.55$ μm we need $a = 0.382$ μm and $r = 0.115$ μm. We now carve out a waveguide by removing air columns. For a rough estimate of the width we should choose, think of the waveguide as an empty space between two perfectly reflecting walls. For the lowest-frequency mode, exactly one-half a wavelength should fit between the walls. This tells us that the width should be roughly $\lambda/2 = 0.77$ μm. We simply remove one row of air columns, see figure 3.3.2.

Figure 3.3.3 shows the band structure for our waveguide. Note that there exist modes in the band gap, which are not allowed in the perfect array. These blue lines corresponds to guided modes, which can travel freely within the narrow waveguide channel. Note that for our waveguide configuration, there are two guided-mode bands. In the insets of the figure are shown the magnetic field patterns of the waveguide modes. The lower band has a more confined structure than the upper band. Furthermore, the modes which are not found in the band gap manifest more dispersive characteristics, because they prefer to concentrate in the periodic region. Note that the field patterns above and below the gap again assures the electromagnetic variational principle.
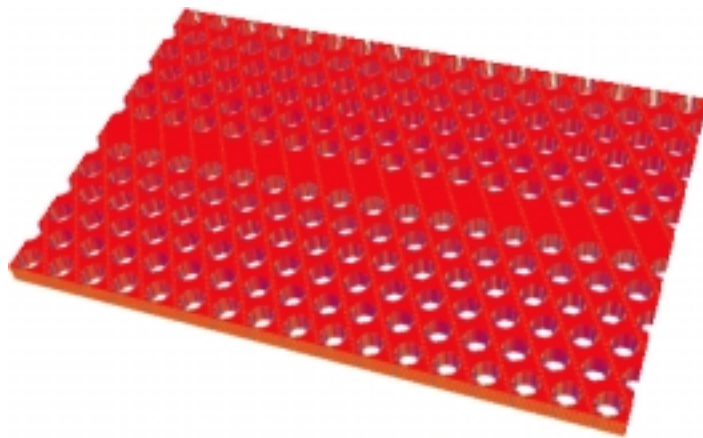
Figure 3.3.2 Designed waveguide formed by removing one row of air columns.
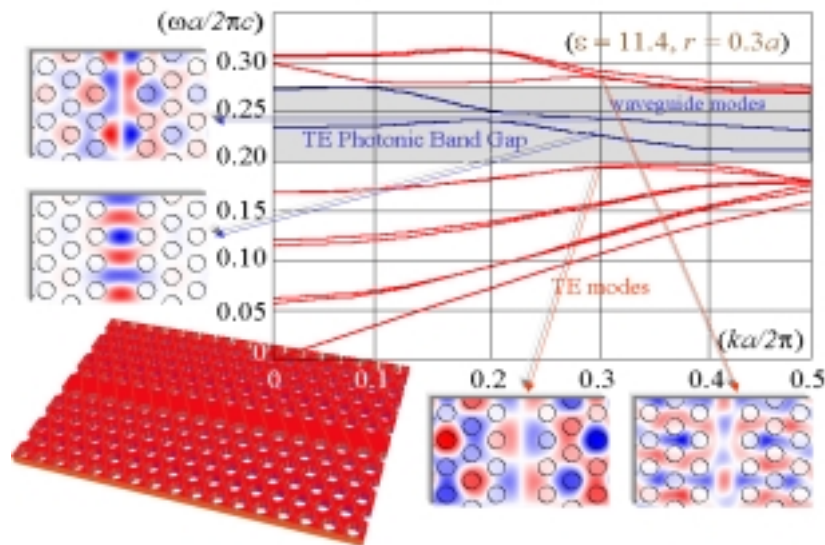
Figure 3.3.3 Photonic band structure for the waveguide.

The radii of the isolated point defects were 0.51a, 0.54a, and 0.57a, respectively. The effect of the isolated point defects in the band structure is shown in figure 3.3.4. Each isolated defect introduces a localized mode (i.e., zero group velocity) in the band structure. These resonant frequencies and their field patterns are calculated with plane-wave expansion and finite-difference time domain method. The insets to the figure will be explained later in this chapter.
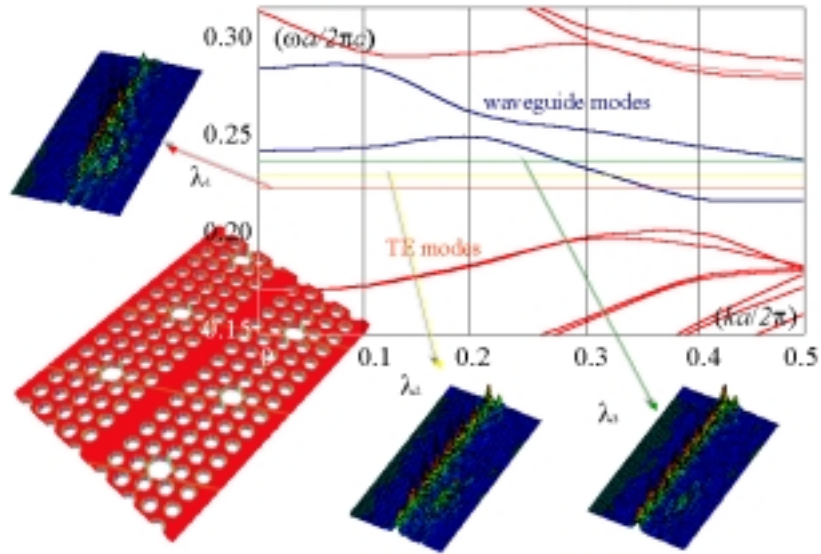
Figure 3.3.4 Effect of the isolated point defects in the band structure.

The spectral behaviour of the slab and the flux of photons, which are trapped from the waveguide and localized in a certain region around the isolated point defects, were studied and calculated using the FDTD method. In our simulation, the input field was defined as a continuous wave with a transverse spatial profile of Gaussian with a mode field diameter of 0.8μm, which is set about equal to the straight waveguide width. The operating wavelength range was tuned by taking central wavelength of 1.55 μm. The radius of the first defect we introduced in the vicinity of the waveguide was 0.51a and the distance between the defect and the waveguide was (3√3/2)a. In this case, we observed that the defect acts as an optical resonator as in Noda et al [1] with a peak wavelength of 1.73 μm. Surface for the intensity of the H_y component of the electromagnetic waves indicating the confinement of photons in the waveguide and localisation around the defect is shown in the left plot of figure 3.3.5. The right plot of figure 3.3.5 illustrates the amplitude of the H_y component in terms of the slices

passing through the defect. Note that around the defect region, all the slices give rise to a peak, which indicates a strong localisation around it.

Defect Size: $r = 0.51a$

Surface plot for the intensity of H_y component of EM field for the defect radius of 0.51 a, corresponding to the resonant wavelength of 1.73 μm.

Amplitude of the H_y component of the field in a.u. for the defect, 0.51 a. The each colored line indicates one slice passing through the isolated point defect.
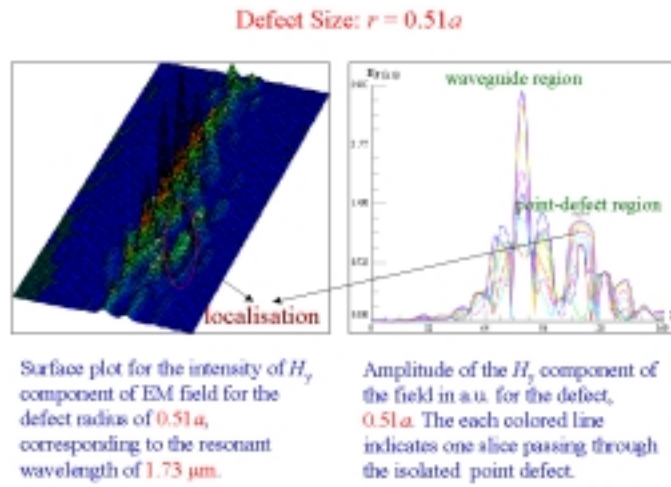
Figure 3.3.5 Confinement and trapping of electromagnetic waves in the waveguide and the isolated point defects in the vicinity of waveguide for the defect radius of 0.51a.

Defect Size: $r = 0.54a$

Surface plot for the intensity of H_y component of EM field for the defect radius of 0.54a, corresponding to the resonant wavelength of 1.699 μm.

Amplitude of the H_y component of the field in a.u. for the defect, 0.54a. The each colored line indicates one slice passing through the isolated point defect.
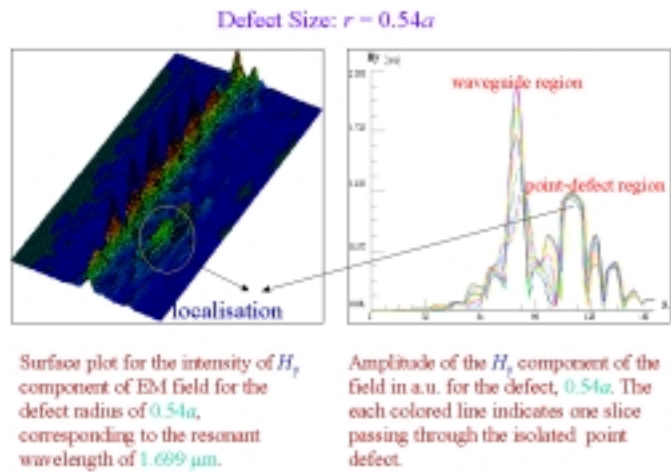
Figure 3.3.6 Confinement and trapping of electromagnetic waves in the waveguide and the isolated point defects in the vicinity of waveguide for the defect radius of 0.54a.

Having shown the trapping and localisation of the photons by the first defect, we next made calculations for a second defect with a radius of 0.54a, which is about 6% larger than that of the first one, and its resonant wavelength is found to be 1.699 μm. From the similar analysis of the third defect with a radius of 0.57a and having the same distance to the waveguide with that of the previous ones; we obtained a resonant wavelength of 1.658 μm. The intensity patterns and the optical field amplitude around the defects are given in figures 3.3.6 and figure

3.3.7. These results show that it is possible to trap and localise photons with different wavelengths by the corresponding defects.

Figure 3.3.8 shows some results. Calculated input and output radiations and coupling ratios, corresponding to the resonant wavelengths in the first column, are illustrated. Second column gives the corresponding defect radii, while the third column indicates the relative power coupling for these defects, which is calculated by the FDTD method, in terms of a constant Γ. In the fourth and fifth columns are given the input radiation in BB radiation form and output radiation, which is emitted from the crystal structure, respectively. Note that the output radiation has a constant scaling factor S, which our method for temperature reading makes use of. Blue colour (last row) indicates the fourth defect, which has a different profile than the others.

Defect size: $r = 0.57a$

localisation

waveguide region

point-defect region

Surface plot for the intensity of H_y component of EM field for the defect radius of 0.57a, corresponding to the resonant wavelength of 1.658 μm.

Amplitude of the H_y component of the field in a.u. for the defect, 0.57a. The each colored line indicates one slice passing through the isolated point defect.
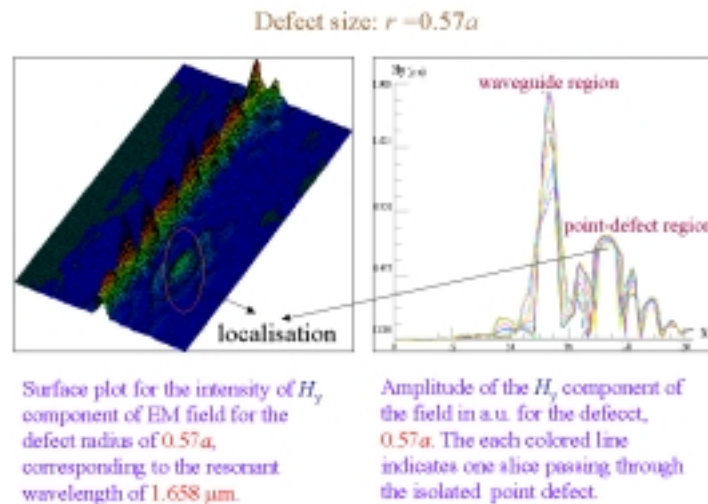
Figure 3.3.7 Confinement and trapping of electromagnetic waves in the waveguide and the isolated point defects in the vicinity of waveguide for the defect radius of 0.57a.

Since the 2D FDTD method is used in our simulations, the effect of finite thickness of the slab, which is rather important in determining the intensity of the photons emitted to free space by the isolated point defects, was not studied. Nevertheless, the properties studied are still powerful enough in explaining the method proposed for the temperature reading of objects. It should also be noted that the defects are studied separately in the simulations, so their dependence to each other is ignored.

In our simulation, followings are also observed: As the radii of the isolated point defects are increased, the resonant wavelengths decrease. This could also be verified in Ref [14], though not stated. Furthermore, we observed that the confined power corresponding to the defects generally becomes smaller as the size of the defects are increased, which is related to the transmission response of the waveguide.

λ (μm)	r (a)	Coup. (Γ)	Inp. Rad. (W/cm².μm)	Out. Rad. (W/cm².μm).S
1.730	0.51	0.95	28.500	27.075
1.699	0.54	1.00	28.775	28.775
1.658	0.57	0.77	29.040	22.361
1.584	0.60	0.49	29.310	14.362

Figure 3.3.8 Some results obtained in the simulation.

After the 2D FDTD analysis of the first three defects, we assumed a fourth defect with a radius of 0.6a, which is about 5% larger than that of the previous ones. It was observed that this later defect does not have a similar coupling profile with the previous three defects. The analysis can be extended over a large number of defects to gain much more about the promising nature of the various useful configurations.

In our calculations, the guided spectrum which forms the optical pulse was centred at 1.55μm be due to the fact that beside performing the temperature field measurement, the device can be employed at the optical communication window for possible potential applications as well. In addition, the normal environment always contains a small but definite amount of carbon dioxide and a variable amount of water vapour. Carbon dioxide strongly absorbs radiation between 4.2 μm and 4.4 μm and the water vapour absorbs strongly between 5 μm and 6 μm and also somewhat in the region 2.6 μm to 2.9 μm [25]. Therefore, these spectral regions should be avoided in the similar designs and simulations. We anticipate that the main drawback of such a practical device, based on the operational principle we introduced here in this paper, would be the detected optical power being very low, and hence, leading a very low signal to noise ratio.

Finally, as the fabrication of such device is concerned, this process can be performed, for example, by the surface micromachining technology [1]. A 2D triangular lattice structure,

with line-shaped and isolated point defects in different diameters, may be drawn on a resist mask coated on the GaAs layer. The resist pattern is then transmitted to the GaAs layer and the substrate under the patterned GaAs layer is selectively etched-off to form the slab structure with isolated point defects and the waveguide.

3.4 Conclusions

In conclusion, a 2D photonic crystal slab structure was designed and simulated for infrared thermometric applications. Such moderate work might highlight potential possibility of using PBG technology in ultra-small IR radiation based devices. A large variety of useful defect resonator configurations remain to be characterised to discover their promising nature. The PBG wavelength range of the 2D slab was designed to be around 1.55 μm region, which makes it also useful as a surface emitting type wavelength-add-drop device, remarkable for division multiplexing in optical communication systems. Furthermore, the strong localisation of the photons at the defect could enhance the nonlinear optical phenomena and trapping of nanoparticles [1]. Future work on defects, taking advantage of their strongly directional behaviour as well as their frequency selectivity and specific polarisation characteristics, will highlight much richer possibilities, provided within a 2D PBG structure environment [20], for many applications such as waveguide bends [29], channel-drop filters [30], optical microelectromechanical systems (MEMS), and perhaps for the quantum computing as well. The results encourage us very much to apply a similar but contrary (not air hole) defect analysis for quantum state transfer between two nodes in a photonic crystal based quantum network, which might be a very useful application towards the next generation quantum communication technology. In the future, we also expect to increase the network capacity by introducing more nodes and controlling photons more extensively.

4. CONCLUSION AND SUGGESTIONS FOR FUTURE WORK

Conclusion and Suggestions for Future Work

A deeper understanding of the properties of materials led to many interesting phenomena in the history of mankind.

In this century, control over the *electrical* properties of the materials and advances in semiconductor physics have allowed us to initiate the transistor revolution in electronics.

In the last decade a new field has emerged with a similar goal: to control the *optical* properties of materials. If we could engineer materials that prohibit the propagation of light, or allow it only in certain directions at certain frequencies, or localize light in specified areas, our technology would benefit. Already, fiber-optic cables, which simply guide light, have revolutionized the telecommunications industry. Lasers, high-speed computers are just a few of the fields next in line to reap the benefits from the advances in optical materials. It is with this goal in mind that this work has been done.

The solution to the problem of optical control and manupulation is thus a *photonic crystal*, a low-loss periodic dielectric periodic medium. In particular, we can design and construct

photonic crystals with photonic band gaps, preventing light from propagating in certain directions with specified energies.

Photonic crystals cannot only mimic the properties of cavities and waveguides but are also scalable and applicable to to a wider range range of frequencies.

Throughout most of the text, I have emphasized the basic principles underlying photonic crystals. By examining a few basic components in detail, I hoped to suggest the practical importance of photonic crystal technology. I believe that the examples described in the work and accomplished in this project are only the tip of a huge iceberg of possibilities in this field that yet to be discovered. My goal in working on this project was to find the way through the quantum network technology, and I am sure that we will benefit much from the photonic band gap materials in the fields including advanced optical interconections, networking in near future and later in the field of quantum information and computation, to turn this tehnology into reality.

APPENDIX A

MPB SIMULATION CODES FOR A LINEAR PC WAVEGUIDE AND A SLAB OF A TRIANGULAR LATTICE OF DIELECTRIC RODS

A1. The following MPB code could be used to calculate the band structure for a linear defect waveguide, which is formed by a row of missing rods along the *x*-direction. The waveguide is based on a a 2D triangular lattice of dielectric rods, with a dielectric constant of 12. Because MPB output files are in the text format, you will need to visualize the structure using appropriate softwares to convert text to picture. Here, *x* and *y* refer to the basis directions in the triangular lattice. For more details, see "Photonic Crystals" by Joannopoulos *et al* [2].

```
(define-param supercell-y 7) ; the (odd) number of lateral supercell
periods

(set! geometry-lattice (make lattice
                (basis1 (/ (sqrt 3) 2) 0.5)
                (basis2 (/ (sqrt 3) 2) -0.5)
                (size 1 supercell-y 1)))

(define-param eps 12) ; the dielectric constant of the rods
(define-param r 0.2) ; the rod radius in the bulk crystal

(set! geometry (list (make cylinder
                (center 0 0 0) (radius r) (height infinity)
                (material (make dielectric (epsilon eps)))))))

(set! geometry
      (append
        ; duplicate the bulk crystal rods over the supercell:
        (geometric-objects-lattice-duplicates geometry)

        ; add a rod of air, to erase a row of rods and form a waveguide:
        (list
  (make cylinder (center 0) (radius r) (height infinity)
        (material air)))))

(define Gamma (vector3 0 0 0))
(define K' (lattice->reciprocal (vector3 0.5 0 0))) ; edge of Brillouin
zone.
(set! k-points (interpolate 4 (list Gamma K')))

; the bigger the supercell, the more bands you need to compute to get
; to the defect modes (the lowest band is "folded" supercell-y times):
(define-param extra-bands 5) ; number of extra bands to compute above the
gap
(set! num-bands (+ supercell-y extra-bands))

(define-param res 32) ; the resolution (grid points/a)
(set! grid-size (vector3 res (* res supercell-y) 1))

; Compute the TM modes, outputting the Ez field in the *middle* of the
; band.  (In general, the guided mode in such an air defect may have
; exited the gap by the time it reaches the edge of the Brillouin
; zone at K'.)
(run-tm
 (output-at-kpoint (list-ref k-points (quotient (length k-points) 2))
          fix-efield-phase output-efield-z))
```

A2. You can calculate the photonic band structure of the a triangular lattice of air holes in a finite-thickness dielectric slab, optionally with a substrate on one side of the slab, with the following MPB code. Mode patterns can also be outputted, however you need to convert the output text to a 3D image first and then visualize using the appropriate 3D visualization software to see the fied pattern. For more details of the structure see "Photonic Crystals" by Joannopoulos *et al* [2]. You can also get many useful information about MPB, and can sign up for the MPB discussion list. See reference [27].

```
; Photonic crystal slab consisting of a triangular lattice of air
; holes in a finite-thickness dielectric slab, optionally with a
; substrate on one side of the slab.  See the paper: S. G. Johnson,
; S. Fan, P. R. Villeneuve, J. D. Joannopoulos, L. A. Kolodziejski,
; "Guided modes in photonic crystal slabs," PRB 60, 5751 (August
; 1999). Mode patterns are also outputted.

; This structure has mirror symmetry throught the z=0 plane,
; and we are looking at k-vectors in the xy plane only.  Thus, we can
; break up the modes into even and odd (analogous to TE and TM), using
; the run-even and run-odd functions.

(define-param h 0.5) ; the thickness of the slab
(define-param eps 11.4) ; the dielectric constant of the slab, GaAs
(define-param loweps 1.0) ; the dielectric constant of the substrate
(define-param r 0.3) ; the radius of the holes
(define-param supercell-h 4) ; height of the supercell

; triangular lattice with vertical supercell:
(set! geometry-lattice (make lattice (size 1 1 supercell-h)
                          (basis1 (/ (sqrt 3) 2) 0.5)
                          (basis2 (/ (sqrt 3) 2) -0.5)))

(set! geometry
      (list (make block (material (make dielectric (epsilon loweps)))
           (center 0 0 (* 0.25 supercell-h))
           (size 1 1 (* 0.5 supercell-h)))
      (make block (material (make dielectric (epsilon eps)))
           (center 0) (size 1 1 h))
      (make cylinder (material air)
           (center 0) (radius r) (height supercell-h))))

; 1st Brillouin zone of a triangular lattice:
(define Gamma (vector3 0 0 0))
(define M (vector3 0 0.5 0))
(define K (vector3 (/ -3) (/ 3) 0))

(define-param only-K false) ; run with only-K=true to only do this k-point
(if only-K
    (set! k-points (list K))
    (set! k-points (interpolate 4 (list Gamma M K Gamma))))

(set! grid-size (vector3 32 32 64))
(set! num-bands 9)
```

```
; Run even and odd bands, outputting fields only at the K point:
(run-even (output-at-kpoint K fix-hfield-phase output-hfield-z))
(run-odd (output-at-kpoint K fix-dfield-phase output-dfield-z))

(display-eigensolver-stats)
```

BIBLIOGRAPHY

[1] Noda *et al*, 2000 *Nature* **407** 608-610.

[2] Joannopoulos *et al*, *Photonic Crystals: Molding the Flow of Light*, Princeton University Press (1995).

[3] http://ab-initio.mit.edu (Joannopoulos' Research Group).

[4] Lin *et al*, 1998 *Nature* **394** 251.

[5] Toader *et al*, Science (2001) **292** 1133.

[6] Omar, *Elementary Solid State Physics*, Addison Wesley Longman (1993).

[7] Guney *et al*, "Design and simulation of photonic crystals for temperature reading of ultra-small structures", 2001 IEEE/LEOS Annual Meeting Conference Proceedings Vol. 1, La Jolla, CA, USA.

[8] Painter *et al*, 1999 *Science* **284** 1819-1821.

[9] Reynolds *et al*, 2001 *Synthetic Metals* **116** 433-437.

[10] Loncar *et al*, 2000 *Journal of Lightwave Technology* **18** 1402-1411.

[11] Johnson *et al*, 1999 *Physical Review B* **60** 5751-5758.

[12] Yablonovitch *et al* 1987 *Physical Review Letters* **58** 2059-2062.

[13] Yablonovitch *et al,* 1989 *Physical Review Letters* **63** 1950-1953.

[14] Kim *et al*, 2001 *Applied Physics Letters* **78** 3015-3017.

[15] Liguda *et al*, 2001 *Applied Physics Letters* **78** 2434-2436.

[16] Culshaw *et al*, 2000 *Physica E* **7** 650-655.

[17] Charlton *et al*, *Materials Science and Engineering B* **74** 17-24.

[18] Sondergaard *et al*, 2001 *Optics Communications* **194** 341-351.

[19] Qiu *et al*, 2000 *Physics Letters A* **266** 425-429.

[20] Smith *et al*, 1998 *IEE Proc.-Optoelectron.* **145** 373-378.

[21] Ho *et al*, 1990 *Physical Review Letters* **65** 3152-3155.

[22] Baker *et al*, 2001 *Agricultural and Forest Meteorology* **108** 281-292.

[23] Qiao *et al*, 1999 *Journal of Applied Physics* **86** 5237-5244.

[24] Cirac *et al*, 1997 *Physical Review Letters* **78** 3221-3224.

[25] Ircon, Technical Solutions, TS104, Introduction to Infrared Thermometry.

[26] Chutinan *et al*, 2001 *Applied Physics Letters* **79** 2690-2692.

[27] Johnson *et al*, The MIT Photonic-Bands Package, http://ab-initio.mit.edu/mpb.

[28] Johnson *et al*, 2001 *Optics Express* **8** 173-190.

[29] Mekis *et al*, 1996 *Physical Review Letters* **77** 3787-3790.

[30] Fan *et al*, 1998 *Physical Review Letters* **80** 96.